

DESCRIPTION OF THE LIULIN TYPE INSTRUMENTS AND MAIN SCIENTIFIC RESULTS

***Tsvetan Dachev, Jordanka Semkova, Borislav Tomov, Yury Matviichuk,
Plamen Dimitrov, Nikolay Bankov, Rositsa Koleva, Stefan Malchev***

*Space Research and Technology Institute – Bulgarian Academy of Sciences
e-mail: tdachev@bas.bg*

Abstract

Ionizing radiation has been recognized as one of the main health concerns for the humans in the near Earth and space radiation environment. The estimation of the radiation effect on health requires at first order accurate knowledge of the accumulated absorbed dose, which depend on the global space radiation distribution, solar cycle and local variations generated by the 3D mass distribution surrounding the space vehicle. This paper presents an overview of the Bulgarian-built spectrometer-dosimeters of Liulin-type and their main scientific results, which was obtained in space, at aircraft, balloon and rocket since 1988.

1. Introduction

The radiation field around the Earth is complex, composed of GCRs, trapped particles of the Earth's radiation belts, solar energetic particles, albedo particles from Earth's atmosphere and secondary radiation produced in the shielding materials around the biological objects [1-4]. Dose characteristics in near Earth and space radiation environment also depend on many other parameters such as the orbit parameters, solar cycle phase and current helio-and geophysical conditions.

1.1. Galactic cosmic rays

The dominant radiation component in the near Earth and free space environment are the galactic cosmic rays (GCR). The GCR are charged particles that originate from sources beyond our solar system. GCR are the

most penetrating of the major types of ionizing radiation. The energies of GCR particles range from several tens up to 10^{12} MeV nucleon⁻¹. The GCR spectrum consists of 98 % protons and heavier ions (baryon component) and 2 % electrons and positrons (lepton component). The baryon component is composed of 87 % protons, 12 % helium ions (alpha particles) and 1 % heavy ions [5]. Highly energetic particles in the heavy ion component, typically referred to as high Z and energy (HZE) particles, play a particularly important role in space dosimetry [2]. HZE particles, especially iron, possess high-LET (Linear energy transfer) and are highly penetrating, giving them a large potential for radiobiological damage [6]. Up to 1 GeV energy, the flux and spectra of GCR particles show modulation that is anti-correlated with solar activity.

1.2. Trapped radiation belts

Radiation belts are the regions of high concentration of the energetic electrons and protons trapped within the Earth's magnetosphere. There are two distinct belts of toroidal shape surrounding the Earth where the high energy charged particles get trapped in the Earth's magnetic field. The inner radiation belt (IRB), located between about 0.1 to 2 Earth radii, consists of both electrons with energies up to 10 MeV and protons with energies up to ~700 MeV. The outer radiation belt (ORB) starts from about 4 Earth radii and extends to about 9-10 Earth radii in the anti-sun direction. The outer belt mostly consists of electrons whose energy is not larger than 10 MeV. The electron flux may cause problems for components located outside a spacecraft (e.g. solar cell degradation). They do not have enough energy to penetrate a heavily shielded spacecraft such as the International space station (ISS) wall, but may deliver large additional doses to astronauts during extra vehicular activity [7-9]. The South-Atlantic Anomaly (SAA) is an area where the IRB comes closer to the Earth surface due to a displacement of the magnetic dipole axes from the Earth's center. The daily average SAA doses reported by Reitz et al., (2005) [10] inside of the ISS vary in the range 74-215 $\mu\text{Gy d}^{-1}$ for the absorbed dose rates and in the range 130-258 $\mu\text{Sv d}^{-1}$ for the averaged equivalent daily dose rates.

1.3. Solar Energetic Particles (SEP)

The SEP are mainly produced by solar flares, sudden sporadic eruptions of the chromosphere of the Sun. High fluxes of charged particles (mostly protons, some electrons and helium and heavier ions) with energies

up to several GeV are emitted by processes of acceleration outside the Sun. It is now generally understood that SEP events arise from coronal mass ejections (CME) from active regions of the solar surface. The CME propagates through interplanetary space carrying along with it the local surface magnetic field frozen into the ejected mass. There is a transition (shock) region between the normal sectored magnetic structure of interplanetary space and the fields frozen into the ejected mass, which forms a transition region (shock) where the interplanetary gas is accelerated forming the SEP. As the accelerated region passes an observation point, the flux intensity is observed to increase dramatically [11]. The time profile of a typical SEP starts off with a rapid exponential increase in flux, reaching a peak in minutes to hours. The energy emitted lies between 15 and 500 MeV nucleon⁻¹ and the intensity can reach 10⁴ cm⁻² s⁻¹ sr⁻¹. Electrons with energies of ~0.5 to 1 MeV arrive at the Earth, usually traveling along interplanetary field lines, within tens of minutes to tens of hours. Protons with energies of 20 to 80 MeV arrive within a few to ~10 hours, although some high energy protons can arrive in as early as 20 minutes. SEP are relatively rare and occur most often during the solar maximum phase of the 11-year solar cycle. In the years of maximum solar activity up to 10 flares can occur, during the years of minimum solar activity only one event can be observed on average [12].

1.4. Atmospheric Ionizing Radiation

The natural radiation level at cruising aircraft altitudes is much higher than it is at ground level. The radiation field arises as a result of the interaction of primary GCR particles with the Earth's atmosphere. An additional flux of albedo secondary GCR is observed at altitudes below 3 km, which contributes to the forming of the flux minimum around 1.6 km altitude [13]. The intensity of the atmospheric radiations, composed of GCR primary and secondary particles and their energy distribution vary with altitude, location in the geomagnetic field, and the time in the sun's magnetic activity (solar) cycle [11]. The atmosphere provides shielding, which depends on the overhead atmospheric depth. The geomagnetic field provides a different kind of shielding, by deflecting low-momentum charged particles back to space. Because of the orientation of the geomagnetic field, which is predominately dipolar in nature, the Polar Regions are susceptible to penetrating GCR (and SEP) particles. At each geographic location, the minimum momentum per unit charge (magnetic rigidity) a vertically

incident particle can have and still reach a given location above the Earth is called the geomagnetic vertical cutoff rigidity [14]. The local flux of incident GCR at a given time varies widely with geomagnetic location and the solar modulation level. When the solar activity is high, the GCR flux is low, and vice versa.

1.5. Natural radioactivity

The larger fractions of the Earth's surface where people live and work has as natural soil cover resulting from weathering processes. The lower atmospheric radiation and the associated external exposure are mainly from gamma rays emitted from the top 25 cm of the surface layer of the Earth and the construction materials of the buildings [15]. At ground level the space radiation (originating from outside the Earth's atmosphere, including solar radiation) generate about 11 % of the effective dose which the average US population, is exposed to, while the terrestrial one (radiation emitted by radionuclides in soil and rocks) is 7 %. The major amount of the effective dose is produced by inhaled Radon and ingested Potassium, Thorium and Uranium [16].

2. Instrumentation

All Liulin type dosimetric instruments use one or more silicon detectors and measure the deposited energy and number of particles into the detector/s when charged particles hit the detector, that allow to calculate the dose rate and particle flux.

The first used in space Bulgarian build dosimetry instrument named LIULIN (see Table 1, Item No 1) was developed for the scientific program of the second Bulgarian astronaut [17].

The measurements in the LIULIN instrument were based on a single silicon detector followed by a charge-sensitive and shaping amplifier (CSA). The number of the pulses at the output of CSA above a given threshold was proportional to the particle flux hitting the detector; the amplitude of the pulses at the output of CSA was proportional to the particles deposited energy and further to the deposited dose. The same measurement procedure was used for the RADIUS-MD instrument (see Table 1, Item No 2). The instrument was developed and qualified for space together with French and Russian colleagues for the unsuccessful Mars-96 mission [18]. LIULIN and RADIUS-MD instruments were designed to

provide data just for the dose rate and particle flux in a single detector, but not data for the deposited energy spectrum. Later this design was no more used, that is why in this paper we will not describe comprehensively it but will summarize the major results obtained during the operation of the LIULIN instrument on MIR space station between April 1988 and September 1994.

Many other instruments was developed and used in space, on ground, aircraft and balloons since then. The paper aims to review the major milestones of their development, calibrations and scientific results.

Table 1 collect information for the all developed and build in Bulgaria instruments that have been used in near Earth radiation environment or around the Moon.

Totally 14 different space instruments were developed, build and qualified for space between 1988 and 2014. 3 of them were lost because of problems with the rockets of the Mars-96, Foton-M1 and Phobos-Grunt missions. R3D-B1 instrument for Foton-M1 mission is not shown in the table because it was very similar to the R3D-B2/B3 instruments for Foton-M2/M3 missions.

The first column of the Table 1 gives information about the name of the satellite, begin and end time and number of available measurements. The second column lists the name of the experiment, Principal investigator (PI) and Co-PIs. Also major references describing the instrument and obtained data are listed. The third column gives the name of the instrument, technical specifications, location, shielding and resolution of the instrument. The last 2 columns present images of the instruments and their locations (carriers).

There are 2 major measurement systems developed by the team till this moment. The first one is based on one detector and is known as Liulin type Deposited Energy Spectrometer (DES) [19, 20], while the second one is dosimetric telescope (DT) by 2/3 detectors [21, 22]).

2.1. DES instrumentation

2.1.1. DES description

The main purpose of the Liulin type Deposited Energy Spectrometer (DES) is to measure the spectrum (in 256 channels) of the deposited energy in a silicon detector from primary and secondary particles at the aircraft and

balloons altitudes, at low earth orbits, outside of the Earth magnetosphere on the route, around and on the surface of the planets of the solar system.

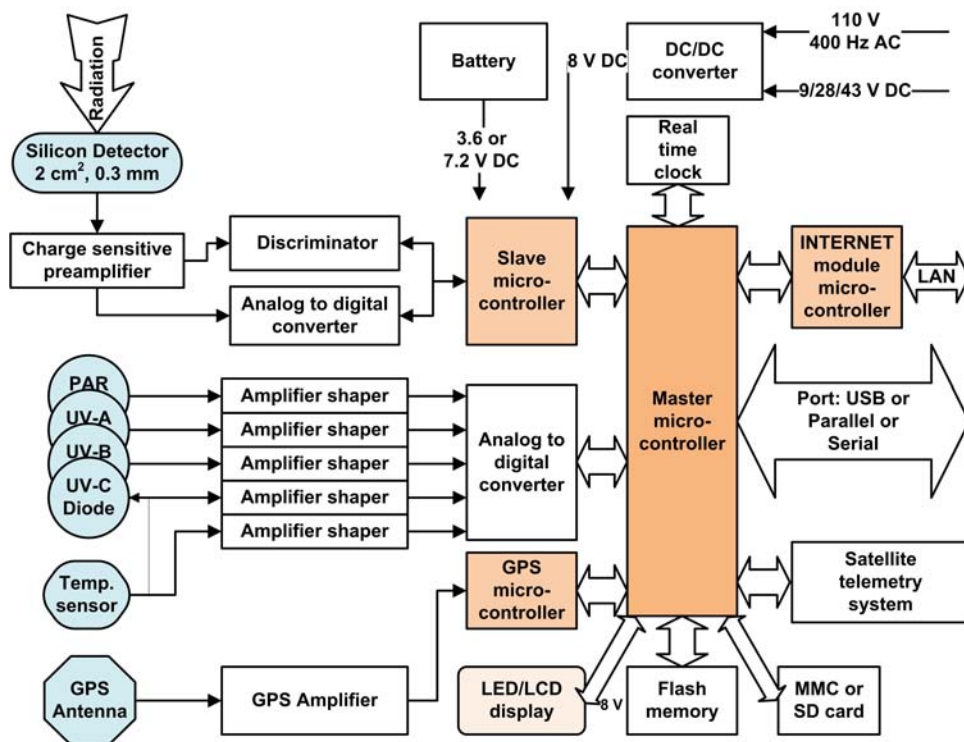


Fig. 1. Generalized block diagram of Liulin-type DES instruments

Historically the first development of DES was for the Liulin-3M instrument [19] for use on aircraft and balloons [23] and for BION-11/12 missions. Later the redevelopment of the Liulin-3M instrument was named Liulin-4 or Liulin-6, which are synonyms of DES.

Fig. 1 presents a generalized block diagram of Liulin type DESs [24]. DES usually contains: one semiconductor detector, one charge-sensitive preamplifier, a fast 256 channel analog-to-digital converter (ADC), discriminator, real time clock, 2 or more microcontrollers and a flash memory. Different modifications of DESs use additional modules such as: UV sensitive photo diodes, temperature sensor, Global Positioning System

(GPS) module with antenna and receiver, LED or LCD display, multimedia card (MMC) or SD card.

Pulse analysis technique is used to obtain the deposited energy from each photon/particle crossing partially or fully the silicon detector. The deposited energies organised in 256 channels form the deposited energy spectrum for each measurement cycle. It is further used for the calculation of the absorbed dose and flux in the silicon detector from primary and secondary particles. The analysis of the shape of the spectrum and the dose to flux ratio, known also as specific dose (SD), permits the characterization of the predominant radiation source in the DES environment [25].

The unit is managed by the microcontrollers through specially developed firmware. The ADC and the slave microcontroller measure organize and keep in RAM memory the 256 channels deposited energy spectrum. The master microcontroller (seen in the right part of Figure 1.) manages the whole work of the spectrometer and data outputs. The developed modifications permits: store of the spectrum data on flash memory or on SD/MMC card; transmission of the spectra data toward parallel, serial or USB port; transmission of spectra data toward internet module and further to LAN network; dose and flux data visualization on alpha numeric or graphic display.

For the two R3D-B2/B3 instruments on Foton satellites and for the R3DE/R instrument on ISS (see Table 1, Item No 4/7 and Item No 9/11), 4 photodiode with filters in different wavelengths and 1 temperature input channels were also developed and used.

Another type of input is the GPS tract, which consists of GPS antenna, receiver and microcontroller unit (MCU). This is used by aircraft instruments for positioning of the measurements versus the geographic longitude, latitude, altitude above the sea level and Universal Time (UT).

Different power supplies were used in the different instruments. They are presented on the upper part of Figure 1 and include 3.6 V or 7.2 V rechargeable or primary batteries, 28 V or 43 V DC aircraft and satellite power and 110 V, 400 Hz AC aircraft power line.

The main measured parameter in the DESs is the amplitude of the pulse after the CSA, generated by a particle or a photon crossing partially or fully the detector [20]. The amplitude of the pulse is proportional by a factor of 240 mV MeV^{-1} to the energy deposited in the detector and to the dose,

respectively. By 8 bit ADC these amplitudes are digitized and organized in a 256-channel deposited energy spectrum.

By definition the dose in the silicon detector D_{Si} [Gy] is one Joule deposited in 1 kg of matter. The DES absorbed dose is calculated by dividing the summarized energy deposition in the spectrum in Joules to the mass of the detector in kilograms:

$$(1) \quad D_{Si} [Gy] = K \sum_{i=1}^{255} (EL_i i) [J] / MD [kg]$$

K is a coefficient. MD is the mass of the detector, and EL_i is the energy loss in Joules in the channel i . The energy in MeV is proportional to the amplitude A of the pulse: $EL_i [MeV] = A [V] / 0.24 [V/MeV]$, where $0.24 [V/MeV]$ is a coefficient dependent on the preamplifier used and its sensitivity.

All 255 deposited dose values, depending on the deposited energy for one exposure time, form the deposited energy spectrum. The energy channel number 256 accumulates all pulses with amplitudes higher than the upper energy-of 20.83 MeV measured by the spectrometer. The methods for characterization of the type of incoming space radiation are described in [25, 26].

2.1.2. DES calibrations

Fig. 2 presents deposited energy spectra from different calibrations of DES, which are compared with proton, electron and GCR spectra obtained at aircraft altitudes and on spacecraft. The individual spectra seen in the figure are obtained after averaging of various numbers of primary spectra and are plotted in coordinates Deposited energy per channel/Deposited per channel dose rate. This allows better understanding of the process of formation of the spectra in the different deposited energy ranges. According to formula (1) the absorbed dose in Si is the area between the curve of the deposited energy spectrum and the abscissa. That is why from bottom to top the spectra position against the ordinate axes depends on the value of the deposited dose rates in Si seen in the legend at the top of the figure.

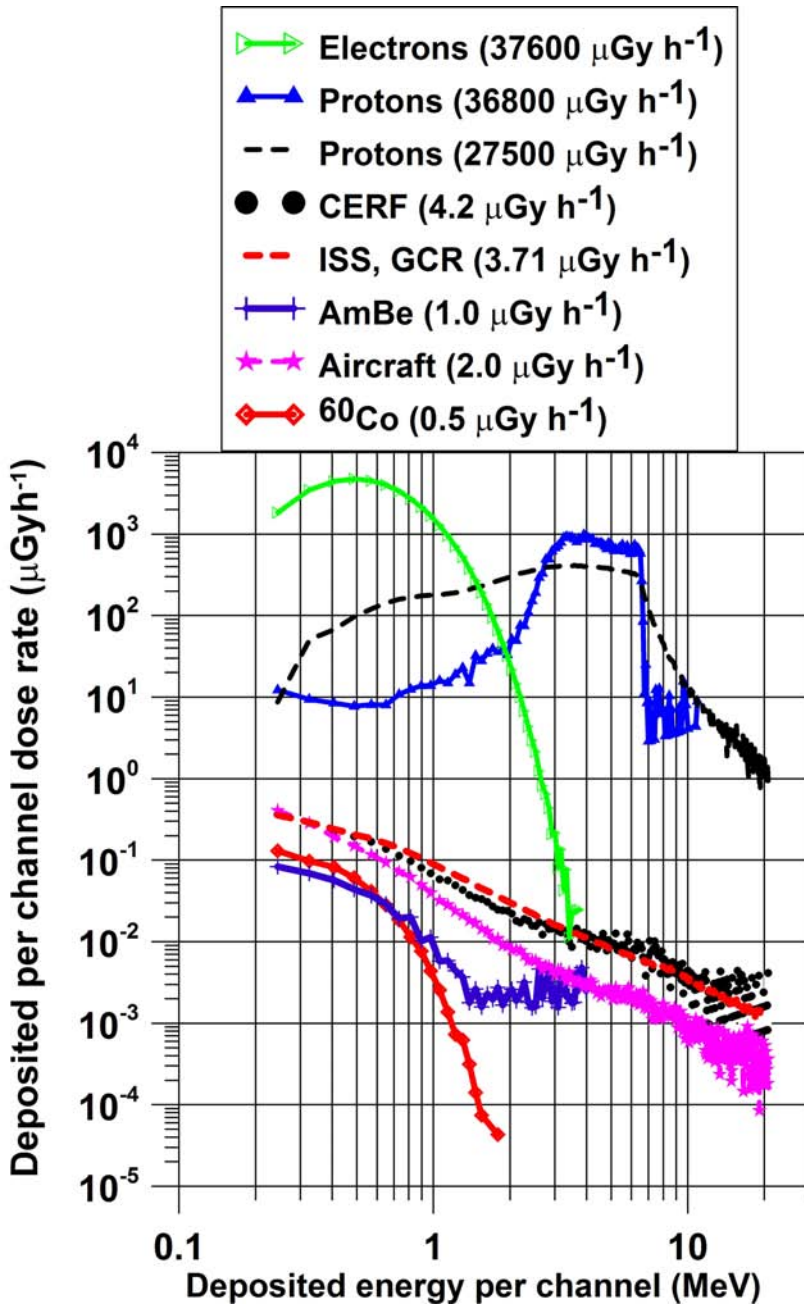


Fig. 2. Different spectrum shapes obtained by Liulin type instruments during calibrations and on aircraft and spacecraft

Lowest diamonds line spectrum in Fig. 2 ($D=0.5 \mu\text{Gy h}^{-1}$) was obtained by Prof. Frantisek Spurny during the calibrations of the Liulin-4C MDU#2 (see Table 2, Item No 1) with ^{60}Co reference radiation source in Nuclear Physics Institute of Czech Academy of Sciences [27]. This spectrum is the shortest because ^{60}Co photons delivered relatively small energy depositions. The absolute values of the dose rates obtained from the spectra are in very good agreement with the dose rates calculated by means of EGS 4 transport code (<http://rcwww.kek.jp/research/egs/>). The values of the measured doses were found to be with 2.8% difference than the reference value for ^{137}Cs source and with 8% difference for ^{60}Co source [27]. The calibrations revealed that except for charged energetic particles, the DES has high effectivity towards gamma rays, which allowed monitoring the natural background radiation.

Next above - crosses line spectrum in Fig. 2 is again by reference radiation source of AmBe emitting neutrons with average energy of 4.4 MeV. This spectrum continues up to about 4 MeV deposited energy with very well seen change of the curve slope around 1.2 MeV deposited energy. The neutrons sensitivity of the DES was further studied in CERN-EU high-energy reference field (CERF) facility [28] on aircraft and in near Earth radiation environment. The spectrum with heavy dots in Fig. 2 is obtained in the CERF facility field, which generates a spectrum containing events in all channels of DES including the 256th channel devoted for energy depositions above the upper level of the spectrometer of 20.83 MeV. The events seen below 1 MeV in AmBe and CERF was supposed to represent the contribution of low LET radiation (electrons, muons, etc), while the events above 1 MeV that of high LET component (neutrons). This idea was further developed and allows from the deposited energy spectrum in the Silicon detector to be calculated the ambient dose equivalent $H^*(10)$ at aircraft altitudes [29, 30].

The CERF energy deposition spectrum is very similar to the averaged aircraft spectrum shown with asterisks line in Fig. 2. This spectrum is obtained by averaging Czech airlines aircraft data during mean solar activity at altitudes close to 10.6 km on routes between Prague and North America towns New York and Montreal [31]. The International Space Station (ISS) R3DE instrument (see Table 2, Item No 5) mean GCR deposited energy spectrum shown with heavy dashed line did have shape even closer to the CERF spectrum. The spectrum was obtained by R3DE

instrument outside ISS by averaging of all measurements with 10 sec resolution for 2418 hours in the period 20 February-31 December 2008 [32].

CERF, ISS and aircraft spectra in Fig. 2 show similar knee around 6.5-7 MeV deposited energy. To explain this knee on Fig. 2 is added the heavy triangle line spectrum ($36800 \mu\text{Gy h}^{-1}$), that was obtained during calibrations of DES (non-shielded detector) with 7.8 MeV protons beam at the Cyclotron facilities of the University of Louvain, Belgium [20]. The knee seen at about 6.3 MeV corresponds to the place where the incident energy of the normally falling to the 0.3 mm thick detector protons is equal to the deposited energy. All normally falling protons, which have smaller energies than 6.3 MeV are stopped inside of the detector. The exact value of the CSDA (continuous-slowng-down approximation) range in g/cm^2 for 0.3 mm silicon is 6.04 MeV [33].

The light dashed line spectrum in Fig. 2 with $27500 \mu\text{Gy h}^{-1}$ absorbed dose rate is obtained by RADOM instrument (see Table 1, Item No 10) on Chandrayaan-1 satellite after averaging of 60 primary 10 seconds resolution spectra [34]. This spectrum shows very similar shape to the cyclotron facilities spectrum shape (see the $36800 \mu\text{Gy h}^{-1}$ full triangle spectrum) and the knee is at the same position. This is so because the energy of the inner belt protons falling on the detector is calculated to be 7-8 MeV e.g. equal to the energy of the cyclotron facilities mono energetic protons falling on the non-shielded detector. Main differences of both spectra are seen in the deposited energy range 0.244 – 2.8 MeV where except protons in space is observed large amount of low LET depositing particles and electrons. Smaller slope of the space spectrum after the knee can be explained with additional amount of ions heavier than protons in space.

The open triangle spectrum is the highest one in Fig. 2. It is obtained on Chandrayaan-1 satellite at altitudes of the ORB (22000 km). This spectrum with predominant electron population is the result of averaging of 120 spectra with 10 seconds resolution. Only the part, in the deposited energies up to 4.0 MeV is shown. Further the spectrum continue with form and shape similar to the ISS GCR spectrum (shown with thick line without symbols in Fig. 2) but here because of the very high count rate of the spectrometer and respectively large dead time the incoming CGR particles are not well detected and presented.

The exact position of the knee depends from the thickness of the detector's shielding and from the exact detector thickness, which are different for the different instruments. As larger these values are as larger is the value of the knee in the spectrum. That is why on Figure 2 the knee is observed above the calculated value of 6.04 MeV in the range 6.0-7.0 MeV. The average value of 6.2 MeV deposited energy is responsible for the channel number 78, which means that all other channels up to 256 of the spectrometer are populated by long pathlength low LET particles (protons) or by neutrons and heavier ions.

More comprehensive the DES calibrations with protons in the Louvain la-Neuve cyclotron facility are presented in [20]. Uchihori et al. in 2002 [35] performed calibrations with protons and heavy ions at Heavy Ion Accelerator at the National Institute of Radiological Sciences (NIRS) in Chiba, Japan (HIMAC) facility in Japan. In both cases of proton calibrations good agreement was found between the measured and the spectra predicted by the GEANT code. Nice coincidence between the predicted and obtained by Liulin-4J (MDU-3) response function was reported by Uchihori et al. [36] (Please see Figure 2 there). The response function was accumulated by points obtained in H^+ , He^+ , $C^+(400\text{ MeV})$ and $Ca^+(400\text{ MeV})$ beams.

The DES effectiveness for neutrons depends on their energy, being minimal for neutrons with energy 0.5 MeV and has a maximum of a few percent for neutrons with energy of 50 MeV in the CERN field [29]. According to the "neutron induced nuclear counter effect" introduced for the Hamamatsu PIN diodes of type S2744-08 (same are used in all DESs) [37] neutrons could be observed in all channels of the spectrum with a probability at least one order of magnitude higher in first 14 channels.

2.1.3. DES data intercomparison with other instruments data

Post-flight calibrations with Liulin-E094 MDUs (see Table 1, Item No 3) were performed in HIMAC heavy ion accelerator during the 1st ICCHIBAN (Inter Comparison for Cosmic-ray with Heavy Ion Beams At NIRS) Project run in Chiba Japan in February 2002 with 400 MeV/u Carbon ions. The deposited energy spectra obtained with all 4 MDUs show a sharp maximum close to 6.1 MeV, that is in good agreement with theoretical prediction and with measurements of the same source with the DOSTEL-1 instrument [38].

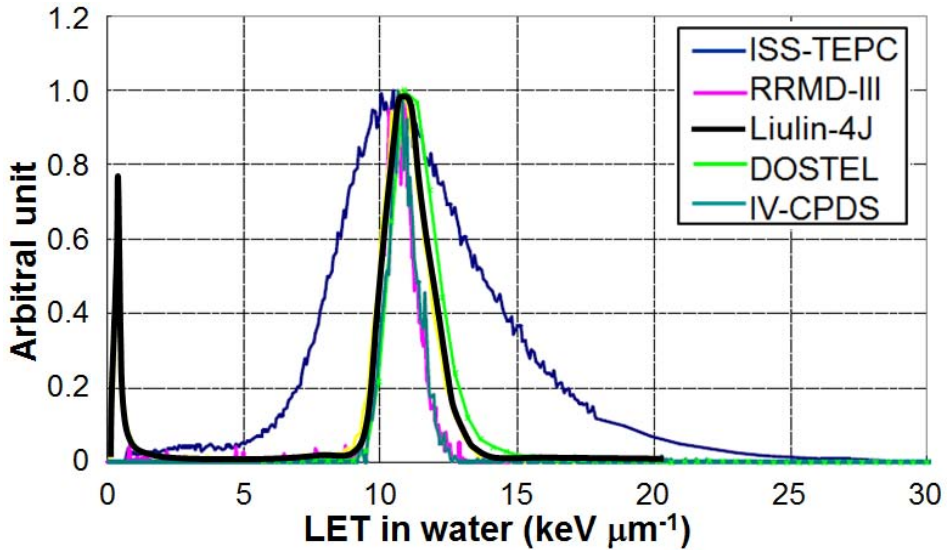


Fig. 3. Comparison of the deposited energy spectra obtained by Liulin-4J instrument with another 3 Si telescopes and ISS-TEPC obtained during the ICCHIBAN-1 test run with 400 MeV/u Carbon ions

Fig. 3 presents comparison of the deposited energy spectra obtained by Liulin-4J instrument (see Table 2, Item No 2) with another 3 Si telescopes (RRMD-III, DOSTEL, IV-CPDOS) and ISS-TEPC obtained during the ICCHIBAN-1 run with 400 MeV/u Carbon ions [39]. It is seen that the silicon detectors show good agreement of LET spectrum. The ISS-TEPC spectrum is wider but it comes from its structure (chord length).

For the purpose of in-space intercomparison between Liulin data with data from another instrument was prepared Fig. 4, which contains data from tissue equivalent proportional counter (TEPC) and 2 Liulin DES instruments - R3DE/R (see Table 1, Item No 9 and 11). The TEPC data are plotted in Fig. 4 using the opportunity provided by Zapp (2013) [40] and by the ‘Coordinated Data Analysis Web’ at the Goddard Space Flight Center (<http://cdaweb.gsfc.nasa.gov/>).

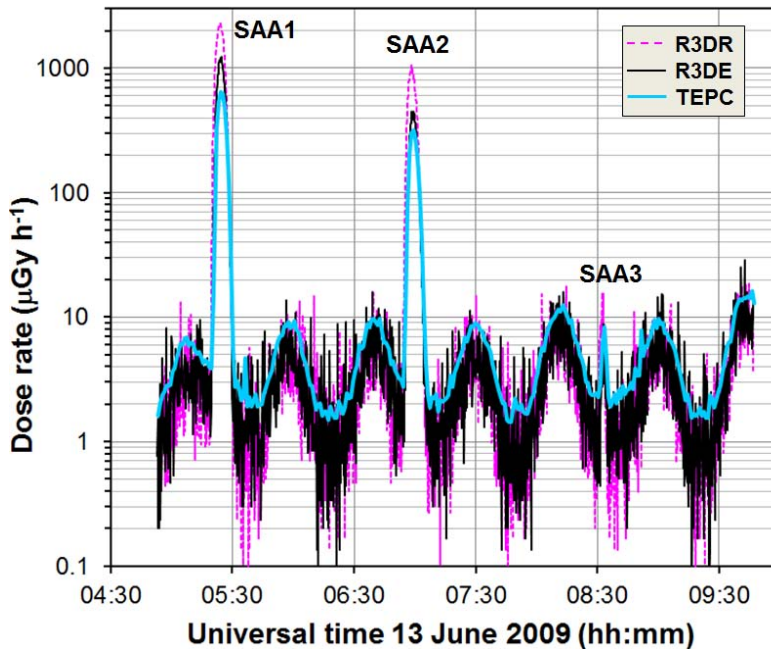


Fig. 4. Comparison of the dose rates measured simultaneously by the R3DE/R instruments and NASA TEPC for a period on 13 June 2009 between 4:53 and 9:46 UT

The dose rate data presented in Fig. 4 is plotted versus the UT and show three passes across the SAA region, which is denoted with labels SAA1-SAA3, seven passes across the high latitude GCR regions in both hemispheres and six passes across the magnetic equator. The analysis of the dose rate dynamics in Fig. 4 shows the following: 1) The R3DR SAA dose rates are the largest and reach $2304 \mu\text{Gy h}^{-1}$ during the SAA1 maximum because R3DR is the lightest shielded instrument [41]. The more shielded by surrounding masses R3DE dose rates are about half that ($1222 \mu\text{Gy h}^{-1}$), whereas the TEPC dose rates (heaviest shielded inside ISS) are the smallest ($645 \mu\text{Gy h}^{-1}$). 2) The TEPC GCR dose rates are higher than the most of the dose rates measured with the R3DE/R instruments. This is because secondary particles build up additional doses in it. In the regions of the magnetic equator the smallest dose rate values are obtained by the R3DR instrument. The R3DE dose rates are in the middle, whereas the TEPC dose rates are the highest. The doses accumulated by the three instruments for 4 h and 56 m are $261 \mu\text{Gy}$ (R3DR), $132 \mu\text{Gy}$ (R3DE) and $100 \mu\text{Gy}$ (TEPC).

DES intercomparison of dose rate measurements on aircraft was performed in a lot of cases. Below in the text we will report some of the more significant.

The exposure of aircraft crew to cosmic radiation has received a great deal of attention after the recommendation by the International Commission on Radiological Protection (ICRP) in 1990, that exposure to cosmic radiation in the operation of jet aircraft should be recognized as occupational exposure, initiated a number of new dose measurements onboard aircraft [42]. In the cited above report there is a large amount of DES dose rate measurements performed by Prof. Frantisek Spurny and compared with other instruments and computer codes, which confirm the ability of DES to characterize the radiation field at aircraft altitudes.

The response of a LIULIN-4 spectrometer was compared by Green et al. [43] to that of the HAWK TEPC <http://www.npl.co.uk/science-+-technology/ionising-radiation/neutron-metrology/hawk-tepc> on 42 aircraft flights in 2003–2004 covering the full range of cutoff rigidity values. On all flights, the absorbed dose measured by both instruments agreed to within 5%. These data provide an in-flight validation of the calibration factor determined by us in ground-based studies.

Getley et al. [44, 44a] performed intercomparison measurements by different detectors including TEPC and Liulin-4SA (see Table 2, Item No 5) on board Boeing 747-400 Qantas Airways flights from August 2008 to March 2009. The flight routes involved cross-equatorial flights between Sydney, Melbourne, and Los Angeles. A northern latitude flight traveled between Sydney, Hong Kong, London, and Singapore, and numerous high southern latitude flights were flown between Sydney and Johannesburg and Sydney and Buenos Aires. In the summary of the paper they wrote: “Comprehensive testing of both the Liulin and QinetiQ QDOS/Rayhound over a 6 month period, at both high northern and southern latitudes as well as in crossequatorial flights, suggests that both of these spectrometers have the ability to provide reliable dose assessments for aircrew monitoring.”

The boxes and additional constructive materials of the most of the DES instruments described in this paper provide between 0.41 and 0.6 g cm^{-2} shielding. For the lower boundary of 0.41 g cm^{-2} shielding the calculated stopping energy of normally incident particles to the detector is 0.78 MeV for electrons and 15.8 MeV for protons [33]. For 0.6 g cm^{-2} shielding these values are 1.18 MeV for electrons and 27.5 MeV for protons. This means

that only protons and electrons with energies higher than the above mentioned values can reach the detector of the instrument.

2.2. Dosimetric telescope (DT) instrumentation

2.2.1. DT description

First application of the Liulin DT method was for the Liulin-5 instrument on ISS. Liulin-5 (see Table 1, Item No 6) is an active experiment in the spherical phantom [45]. The aim of Liulin-5 experiment is long-term investigation of the depth-dose distribution and continuous monitoring of the particle fluxes, dose rates, energy deposition and LET spectra in a radial channel of the Russian spherical tissue-equivalent phantom MATROSHKA-R [46, 47], using a telescope of three silicon detectors. Liulin -5 is sensitive to photons, electrons, protons and heavy ions. Liulin-5 charged particle telescope was launched to ISS by Progress-60 cargo craft in May 2007.

The investigation of the radiation environment in the phantom on ISS by Liulin-5 experiment envisages: i) measurement of the depth distributions of the energy deposition spectra, flux and dose rate, and absorbed dose D ; ii) measurement of the LET spectrum in silicon, and then calculation of LET spectrum in water and Q , according to the $Q(L)$ relationship given in ICRP – 60, where L stays for LET. $Q(L)$ is related functionally to the unrestricted LET of a given radiation, and is multiplied by the absorbed dose to derive the dose equivalent H . H , D and Q are related by:

$$(2) \quad H = Q_{av}D ,$$

where D is the absorbed (integrated over all particles) dose, and Q_{av} is the dose averaged quality factor, given by:

$$(3) \quad Q_{av} = \int Q(L)D(L)dL / D$$

Liulin-5 consists of two units: a detector module and an electronics module (see Table 1, Item No 6). The detector module is mounted in the radial channel of the phantom, while the electronics is outside the phantom. More detailed description of Liulin-5 method and instrument can be found in [45, 48]. The detector module contains 3 silicon detectors (D1-D3) arranged as a particle telescope.

Fig. 5 is a schematic diagram of Liulin-5 and the spherical phantom. The sensitive thickness of the detectors D1 and D3 is 370 μm , of D2 it is 360 μm and the detectors' diameter is 17.2 mm. The D1 detector is placed at 40 mm depth in the phantom, D2 is at 60 mm and D3 is at 165 mm distance from its surface.

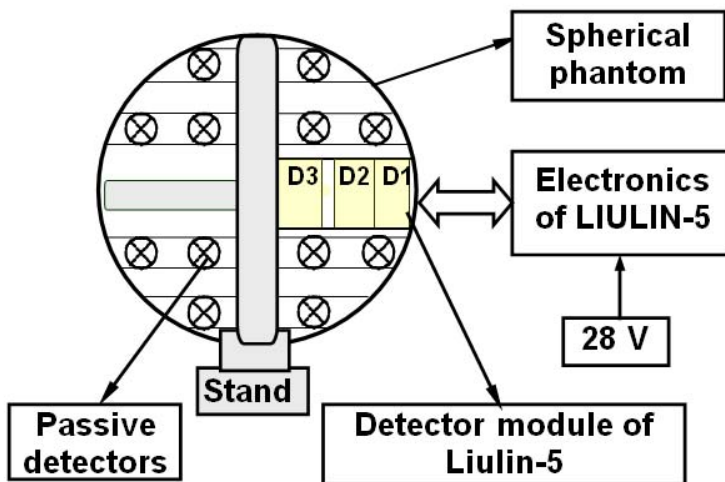


Fig. 5. Schematic diagram of Liulin-5 experiment in the spherical phantom

From each detector the energy deposition spectrum for a cycle of measurement is recorded in two 256 channels' sub-ranges. Then the overall energy deposition spectrum is constructed in 512 channels. The amount of energy ΔE deposited in the detector is proportional to the value $k1\sum(iN_i)+k2\sum(jN_j)$, and the incident particle flux is proportional to $\sum N_i+\sum N_j$. Here i and j are the spectral channel numbers in the two sub-ranges (LLET and HLET), N_i and N_j are the amount of particles registered in channels i and j of the corresponding sub-ranges, $k1$ and $k2$ are coefficients. The values $\sum(iN_i)$, $\sum(jN_j)$, $\sum N_i$, $\sum N_j$ are recorded for given time intervals and are used for calculation of the doses and particle fluxes rates.

The absorbed dose in the detector is calculated as

$$(4) \quad D = \Delta E/m,$$

where m is the detector's mass.

The geometry factor for converting the measured in a single detector amount of particles into differential flux is $14.6 \text{ cm}^2 \text{ sr}$, assuming the incident flux is isotropic.

Detectors D1 and D2 operate in coincidence mode. The distance between D1 and D2 is 20 mm. The viewing angle of D1-D2 assembly is 81.4° . When a particle enters the telescope within the 81.4° -degree sensitivity cone, with energy enough to make it through both the D1 and D2 detectors, it is considered a coincident event. The energy deposition spectrum measured in the D1 detector in coincidence mode with the D2 is recorded and used to obtain LET spectrum. Since the incidence angle of the particles is not measured, the energy deposition is converted into mean LET in silicon as:

$$(5) \quad \text{LET}(\text{Si}_i) = \Delta E_i / h_{D1},$$

where ΔE_i is the deposited energy in channel i , $\text{LET}(\text{Si}_i)$ is the LET in silicon in channel i (here $i = 1-512$), and h_{D1} is the D1 thickness. Calculations show that the dependence of the telescope's effective area on particle incident angle is practically linear and decreases from 2.324 cm^2 at 0° between the telescope axis and flux to 0 cm^2 at 40.7° . The average increasing of particle range in the detector in case of nonparallel to the axis incidence is 7 %.

The LET spectra in silicon obtained are used for calculation of the differential and integral LET spectra in water, the absorbed dose rates and the quality factors. The geometry factor for converting the measured by the D1-D2 telescope amount of particles into differential isotropically incident flux is $2.01 \text{ cm}^2 \cdot \text{sr}$. The energy deposition in water (tissue) relative to that in silicon is taken to be 1.24, independent of particle energy. LET for water $\text{LET}(\text{H}_2\text{O})$ is then found by the following relation:

$$(6) \quad \text{LET}(\text{H}_2\text{O}) = 1.24 \times \text{LET}(\text{Si}) / 2.34$$

Taking into account that the relation between $\text{LET}(\text{H}_2\text{O})$ and $\text{LET}(\text{Si})$ changes with proton energy E_p from 1.27 for $E_p = 30 \text{ MeV}$ to 1.21 for $E_p = 1000 \text{ MeV}$, and that for a typical energy $E_p = 100 \text{ MeV}$ the conversion coefficient is 1.24, the maximum difference of $\text{LET}(\text{H}_2\text{O})$ obtained by using real conversion function and the simple conversion factor is less than 3 %.

To obtain the LET spectrum dose of isotropically incident particles, the dose calculated from the D1-D2 coincidences spectrum is multiplied by 13.5.

The instrument provides time resolved: Absorbed dose rate in each detector; Flux rate in the range $0 - 4 \times 10^2 \text{ (cm}^2 \text{ s}^{-1}\text{)}$, measured in each of the detectors; Energy deposition spectra in D1 detector in the range 0.45-63 MeV in 512 spectral channels; Energy deposition spectra in D2 detector in the range 0.45-60 MeV in 512 spectral channels; Energy deposition spectra in D3 detector in the range 0.2-10 MeV in 512 spectral channels; LET(H₂O) spectra in the range 0.65-90 keV μm^{-1} in 512 spectral channels. The events exceeding the upper energy deposition or LET limit of each detector are recorded in the corresponding 512-th channel.

Second application of the DT method was for the Liulin-Phobos instrument (see Table 1, Item No 12) developed for the Phobos-Grunt mission [22]. The main goal of the Liulin-Phobos experiment was the investigation of the radiation environment and doses in the heliosphere at distances of 1 to 1.5 AU from the Sun and in the near-Mars space.

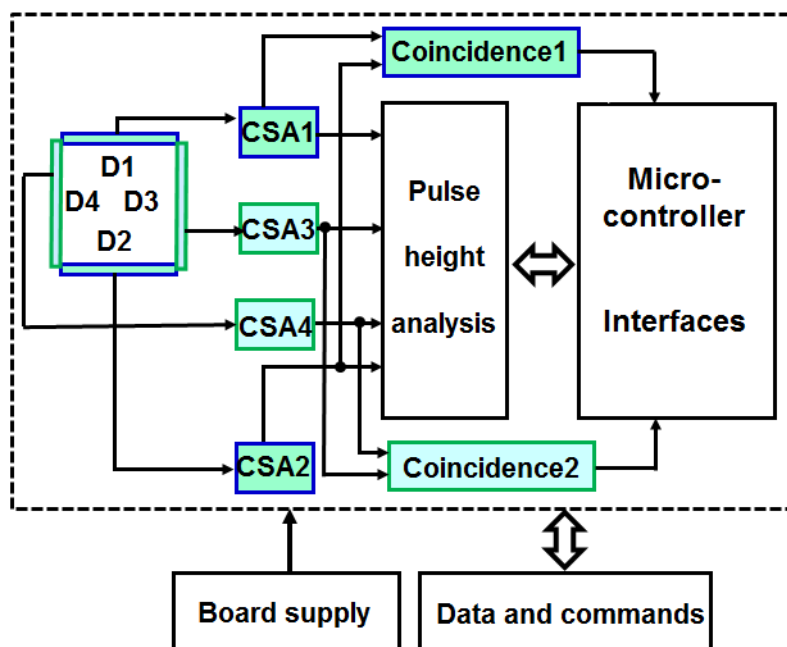


Fig. 6. Block-scheme of Liulin-Phobos charged particle telescope

Liulin-Phobos instrument consisted of two dosimetric telescopes - D1&D2, and D3&D4 arranged at two perpendicular directions. The block-schema of the instrument is shown in Fig. 6. Every pair of telescopes consists of two 0.3 mm thick Si PIN photodiodes, operating in coincidence mode to obtain LET. One of the detectors in every telescope measures the energy deposition spectrum in the range 0.1-10 MeV, and the other in the range 0.45-90 MeV. In that way every dosimetric telescope provides data in the energy deposition range 0.1 - 90 MeV. The instrument was designed to measure absorbed dose rate and particle flux every 60s, energy deposition spectra and LET spectrum every 60 min.

The parameters featured by Liulin-Phobos DT was: Absorbed dose rate in the range 4×10^{-8} -0.1 Gy h⁻¹, and absorbed dose D, measured by every single detector; Particle flux in the range 0-10⁴ cm⁻² s⁻¹, measured by every single detector; Energy deposition spectra in the range 0.1-90 MeV, measured by every dosimetric telescope; LET spectrum (in H₂O) in range 0.75–155 keV/μm, measured by every DT; Quality factor Q = f(LET) and average quality Q_{av}; Dose equivalents H = Q_{av} D, measured by two DT.

A similar to the Liulin-Phobos DT instrument is now under development for the ExoMars mission [49].

2.2.2. DT calibrations

Liulin-5 was exposed to 400 MeV/n ¹⁶O and 300 MeV/n ⁵⁶Fe beams during the ICCHIBAN-7 experiments [50] at the HIMAC in September 2005.

Fig. 7 shows the deposited energy distribution in the silicon detectors of Liulin-5 obtained during the exposures to 400 MeV/n ¹⁶O [45]. At first the detector module of Liulin-5 was exposed perpendicular to the beam with beam center at the center of the detectors (0° inclinations). After that detector module of Liulin-5 was inclined at angles of 30° and 60° relative to the beam line and rotation was made around the centre of D1 detector. On each plot two distributions are seen – the left represents measured spectra in LLET range and the right represents measured spectra in HLET range of the detectors. We assume that HLET peaks correspond to the distribution of the main ¹⁶O beam, and the LLET peaks correspond to scattered background beams. Most of HLET events registered in D3 detector exceed the upper energy loss range limit of that detector and were registered in the highest spectral channel as events of 10 MeV.

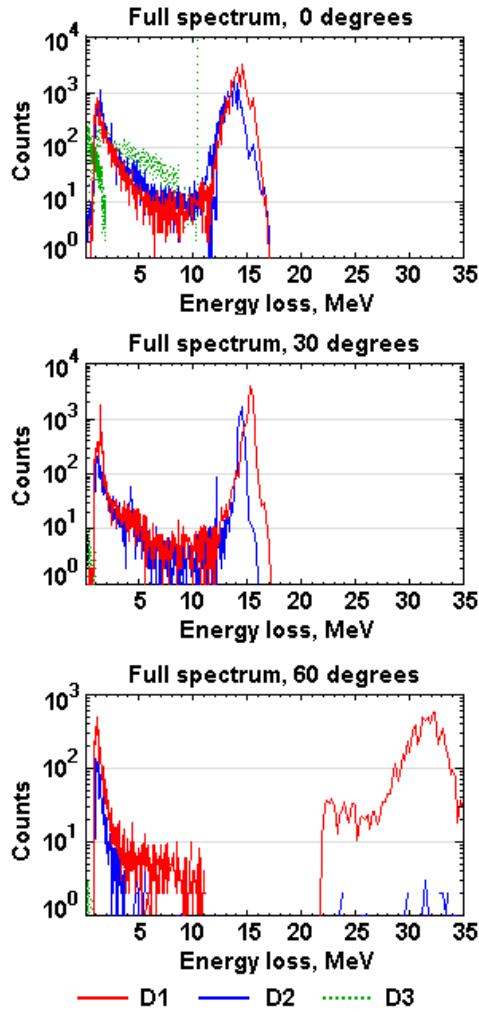


Fig. 7. Deposition energy distributions of ^{16}O beam in the silicon detectors D1–D3 of Liulin-5

For the 30° exposure D3 detector was outside the main beam, and for the 60° exposure both D2 and D3 detectors were outside the main beam. That is why only scattered background beams in LLET ranges were registered in them.

As a result of the calibrations the Liulin-5 measurement range of LET(H₂O) was estimated to be 0.65 –90 keVμm⁻¹. This makes it possible for Liulin-5 to measure the low-LET components of cosmic radiation, as well as a significant part of biologically relevant high-LET heavy ion component of GCR that contribute to the radiation doses on ISS.

The Liulin-Phobos flight unit was calibrated with proton and heavy ion beams at the cyclotron and at the HIMAC accelerator at the NIRS, Japan in January-February 2009. The calibrations were performed in agreement with the Memorandum of Understanding on collaboration concerning development, calibration, space flight measurements and data analysis of the Liulin-F instrument onboard the Phobos-Soil mission, which was signed between STII-BAS, IBMP-RAS NIRS, Chiba, Japan.

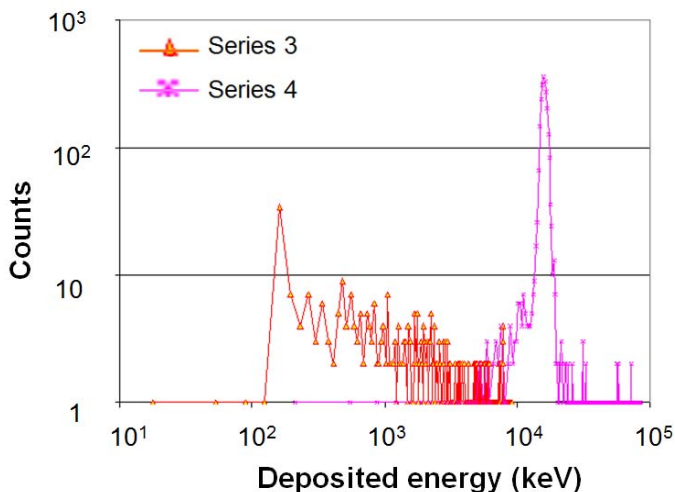


Fig. 8. LET spectrum of ²⁰Ne 600 MeV/u, obtained in D1&D2 telescope at 0° inclination of the telescope axis to the incident beam

As an example of the obtained results Fig. 8 shows the energy deposition spectrum in the D2 detector in a coincidence mode with D1 (LET spectrum) of ²⁰Ne ions with energy 600 MeV/n [51]. The distribution was obtained at 0° inclination of the telescope's D1-D2 axis to the ion beam. The left part of the LET distribution was measured in low LET range of the detector and is mainly due to secondary radiation, resulting from interactions of primary neon beam with surrounding materials. The main peak represents the LET distribution of the neon ions and was measured in high LET range of this detector. The obtained LET(H₂O) of ²⁰Ne 600

MeV/n is 26.7 keV/ μm –it is in good agreement with the theoretically calculated value of 25.5 keV/ μm , having in mind the shielding of the detectors. The results of the Liulin-Phobos calibrations at NIRS confirm the correctness of the electronic calibrations made preliminary.

3. Main experiments and results in space

3.1. LIULIN experiment on MIR space station

The Bulgarian-Russian dosimeter-radiometer LIULIN (see Table 1, Item No 1) was installed in the working compartment of the MIR space station [17]. The effective mass thickness of screening matter inside the working compartment of MIR is evaluated to be 6-15g cm⁻². Thus the main contribution to the count rate is given by protons and electrons that, outside MIR space station, have energy large than 100 MeV and 10 MeV respectively. It uses a silicon detector with a thickness of 306 microns and area of 1.8 cm². Simultaneous measurement of the energy absorbed in the detector and of the flux of particles are recorded and transmitted to Earth. The noise level of the detector and electronics was 83 keV. The dose sensitivity is 1 nGy/pulse. The detector unit (see Table 1, Item No 1) is a miniature, portable, self-indicating devise. LIULIN-Microcomputer unit (MCU) is an eight-bit microprocessor unit.

Main results obtained by the LIULIN device can be listed as follows:

- During the declining phase of 22nd solar cycle the GCR fluxes observed at $L > 4$ have been enhanced from 50-70 $\mu\text{Gy day}^{-1}$ in 1989-1990 up to 130-140 $\mu\text{Gy day}^{-1}$ in 1993-1994. In same time the GCR flux increased from an average value of 0.58 cm⁻² s⁻¹ in 1991 up to 1.53 cm⁻² s⁻¹ in 1991 [52];
- The peak value of the dose rate and flux of particles measured by LIULIN in the SAA increase gradually by a factor of 2 between 1991 and 1994 at the altitude of 410 km. The increase is attributed to the decrease of the atmospheric density during the declining phase of solar activity, which is due to the lower rate of heating of the upper atmosphere when the solar UV and EUV radiation diminishes during the minimum of solar cycle A power law relationship has been deduced between local atmospheric density at the altitude of MIR station and the maximum dose rate in the center of the SAA when the neutral density decreased from 8×10^{-15} g cm⁻³ to 6×10^{-16} g cm⁻³ the maximum dose increases from 200 to 1200 mGy h⁻¹, while the flux of particles increased from 30 to 120 cm⁻² s⁻¹ [52];

- LIULIN measurements represent the low altitude manifestation of radiation belts dynamics. Before the 23-26 March 1991 solar-geomagnetic events LIULIN dose and flux data exhibited one maximum located at $L \sim 1.4$ the region of the SAA. It is due to the particles from the inner radiation belt. After the March 23 1991 geomagnetic storm a “new” maximum in LIULIN flux data was created at $1.8 < L < 2.2$. This was an unique phenomenon, not reported previously and after http://www.stp.isas.jaxa.jp/akebono/RDM/rdm/rdmflux_1989_2010.gif. It was a relatively stable configuration observed during the whole of 1991 independently of the geomagnetic conditions. It was identified in LIULIN data till the middle of 1993. The outer radiation belt maximum was frequently observed after geomagnetic disturbances as a dynamic structure for 1-3 months. ORB in MIR data was usually located at $2.5 < L < 3.2$. After long quiet conditions it disappeared [53];
- Several outstanding SEP took place during the LIULIN observations. SEP data are available for September 29, 1989, October 18, 1989, March 23, 1991, June 8 and 15, 1991, and June 26, 1992. Data analysis of them is presented in the paper by Shurshakov et al. [54].

3.2. Experiments and results on ISS

The largest amount of Liulin experiments in space since 2001 was performed on ISS. Listing them we have to mention: Liulin-E094 (April-August 2001), Liulin-ISS (September 2005-till now), Liulin-5 (May 2007-till now), R3DE (February 2008-September 2009) and R3DR (March 2009-August 2010) (see Table 1, Items No 3, 5, 6, 9, 11). Two of them Liulin-ISS and Liulin-5 are working until now. R3DR experiment is scheduled to be repeated as part of EXPOSE-R2 mission for 1.5 years since June 2014 at Russian Zvezda module of ISS http://www.nasa.gov/mission_pages/station/research/experiments/211.html.

3.2.1. DES data selection procedure

The data selection procedure was established for DES instruments to distinguish between the three expected radiation sources: (i) GCR particles, (ii) protons with more than 15.8 MeV energy in the SAA region of the IRB and (iii) relativistic electrons with energies above 0.78 MeV in the ORB [25].

Fig. 9 is prepared to confirm these features with the R3DR data. The abscissa plots the measured flux in $\text{cm}^{-2} \text{s}^{-1}$, while the ordinate shows the dose rate in $\mu\text{Gy h}^{-1}$ and dose rate to flux ratio (D/F) (or specific dose SD) in $\text{nGy cm}^{-2} \text{particle}^{-1}$ [25, 55] for the period 1 April–7 May 2010, which is remarkable with very high ORB fluxes and respectively dose rates [8]. The large amount of experimental points (295374 points) in the diagonal of the figure is responsible for the dose rate values, which, as expected, are in linear dependence from the flux, while the almost horizontally plotted points present the D/F ratio.

Three branches in each graphic are differentiated and they look as a left hand wrist with two fingers. The wrist represents a highly populated part in the diagonal bunch of points: (1) it takes a large amount of the measured points in the range $0.03\text{--}30 \mu\text{Gy h}^{-1}$; (2) for a fixed flux a wide range of doses is observed. These two features could be explained only by the GCR particles, which, being with small statistical relevance and high LET, are able to deposit various doses for fixed flux value. The smallest dose rates ($0.03\text{--}0.4 \mu\text{Gy h}^{-1}$) are observed close to the magnetic equator, while the largest are at high latitudes. In the horizontal graphic this part of the data is represented with a similar large amount of points, which in large scale overlap the dose rate diagonal points.

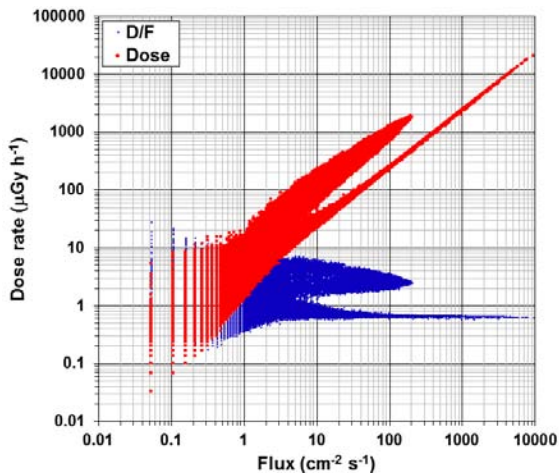


Fig. 9. Characterization of the R3DR predominant radiation sources by the dose rate from flux and dose to flux (D/F) dependencies

The “index” finger is in the dose rate range 9–22,000 $\mu\text{Gy h}^{-1}$ and looks as a straight line. Its representation in the horizontal graphic is a finger extending up to 10,000 in $\text{cm}^{-2} \text{s}^{-1}$, with dose to flux values below 1 $\text{nGy cm}^{-2} \text{particle}^{-1}$. This finger is based on low LET particles and could be formed only by the relativistic electrons [7] in the outer radiation belt.

The “big” finger in the diagonal graphic has a different source compared to the previous two because it is characterized by a high range of doses for fixed flux but the dose rates are in the range 30–1900 $\mu\text{Gy h}^{-1}$. This amount of points could be formed only by protons from the IRB (The region of South Atlantic Anomaly (SAA)) whose dose depositions depend on the energy. The lower energy protons are depositing higher doses. In the horizontal graphic this finger has a similar form and is situated in the range 1.2–8. $\text{nGy cm}^{-2} \text{particle}^{-1}$. Both IRB and ORB fingers can be approximated by straight lines. From these approximations we obtain that 1 proton in IRB produces in the Silicon detector on average a dose of 1.4 nGy , while 1 electron in ORB produces a dose of 0.33 nGy , which is in good agreement with Heffner’s formulae [55].

The conclusion which can be drawn from Fig. 9 is that the data can be simply split in two parts by the requirements for the ratio $D/F < 1$ and $D/F > \text{nGy cm}^{-2} \text{particle}^{-1}$. This will generate graphics, which will divide the IRB and ORB sources. GCR protons in equatorial and low latitude regions have very small fluxes of less than 1 $\text{particle cm}^{-2} \text{s}^{-1}$, that is why the D/F ratio is not stable and varies in the range from 0.03 to 30 $\text{nGy cm}^{-2} \text{particle}^{-1}$ [8]. This variation makes the D/F ratio inapplicable for the characterization of the GCR radiation source.

3.2.2. Liulin-E094 results

The first use of DES in space was in the Liulin-E094 instrument (see Table 1, Item No 3), that was developed, qualified for space and used in the ESA Dosimetric Mapping-E094 experiment [10] on the US Laboratory module of the ISS as a part of the Human Research Facility in May-August, 2001 [18]. The main purpose of this experiment was to investigate the dose rate distribution inside the US Laboratory module and Node-1 of ISS.

In the paper by Dachev et al., 2006 [56] was developed a 3-D shielding model of the MDU unit and located it at the four locations in the ISS shielding model. Using the trapped proton differential spectra generated from the SPENVIS on-line capability for calculation of AP8 trapped proton

spectra and the high-energy proton transport code PDOSE we was able to calculate the doses at each locations of MDUs. The differences between the observed Liulin-E094 MDUs doses and calculated do not exceed 15%. The obtained data were also used for statistical validation of the high-charge and energy (HZE) transport computer (HZETRN) code [57-59].

3.2.3. Liulin-ISS results

Liulin-ISS instrument (see Table 1, Item No 3) was launched to the Russian segment (RS) of ISS in September 2005. It contains four Mobile Dosimetry Units (MDU) with displays and Control and interface unit and was used in the Service Radiation Monitoring System of the RS of ISS [60]. Following information may be displayed: Current dose in $\mu\text{Gy h}^{-1}$, Current event rate (Flux) $\text{cm}^{-2} \text{s}^{-1}$, Accumulated from the “Switch ON” dose mGy. The battery operation time of the MDU is about 7 days. The 4 MDU can be used as personal dosimeters in case of dangerous SEP. Because some problems with the telemetry system connections the instrument was not used as planned and now under development is a new instrument with similar functions, which is expected to be in space in the next 2-3 years.

3.2.4. Liulin-5 results

Liulin-5 DT instrument (see Table 1, Item No 5) [21] was launched to the RS of ISS in May 2007. Measurements with Liulin-5 were conducted in the spherical tissue equivalent phantom of Matroshka- R experiment located in the PIRS-1 module of ISS in the period July 2007 – March 2010, corresponding to the minimum of solar activity in 23rd solar cycle. Also measurements corresponding to the maximum of 24th solar cycle have been conducted since December 2011 till now (April 2014) both inside and outside the phantom located in the MIM1 module of ISS. The main results obtained during the minimum of 23rd solar cycle were published in [61-63]. (Semkova et al., 2012, 2013a, 2013b)

During the SEP events of 7-12 March 2012 (see Fig. 10) at $L > 3$ the particle flux and dose rates increased in all three detectors of Liulin-5 charged particle telescope located at 40, 60 and 165 mm depths along the radius of the tissue-equivalent spherical phantom in MIM1 module of ISS [63a].

The additional absorbed dose at 40 mm depth in the phantom received from SEP event on 7-9 March 2012 was approximately 180 μGy . The additional dose equivalent at 40 mm depth in the phantom received

from that event was about 448 μSv . The additional exposures received from SEP event are comparable to the average daily absorbed dose and dose equivalent measured in the spherical phantom in ISS during quite periods.

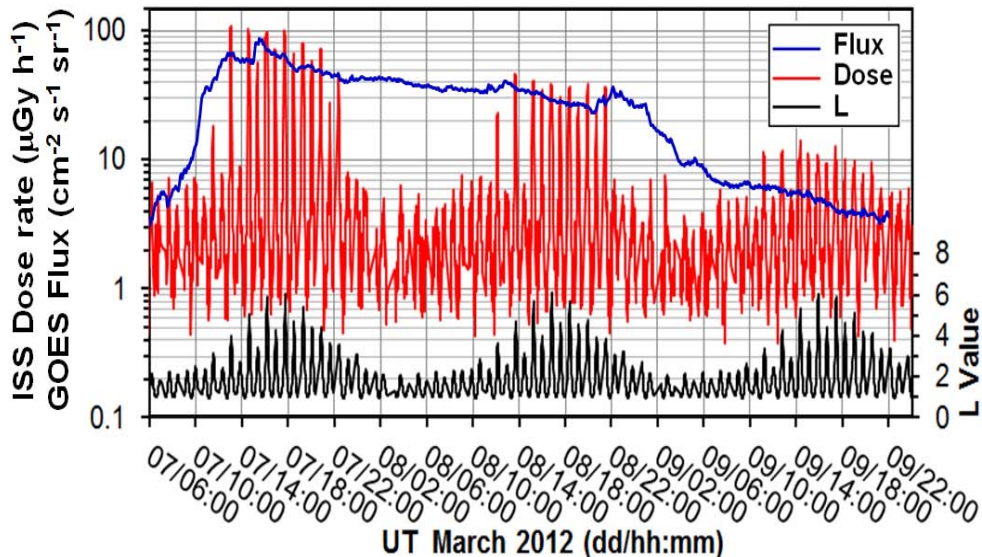


Fig. 10. Proton flux with energies ≥ 100 MeV measured by GOES-13 (blue curve), the dose rate in D1 detector of Liulin -5 measured outside the SAA (red curve), and the corresponding L-values (black curve) versus time during the March 2012 SEP event

In Figure 10 it is seen that there is a good agreement of Liulin-5 dose rates trend during the SEP event with the proton flux of energies ≥ 100 MeV (able to penetrate inside ISS) measured by GOES – 13 satellite (blue line).

3.2.5. R3DE instrument results

R3DE instrument (see Table 1, Item No 9) with 256 channels ionizing radiation monitoring spectrometer and 4 channels UV spectrometer worked on the ESA European Technology Exposure Facility (EuTEF) platform inside of EXPOSE-E facility outside of the European Columbus module of the ISS between 20 February 2008 and 1 September 2009 with 10-s resolution behind 0.45 g cm^2 of shielding [25, 32].

There are 2 major discoveries connected with the R3DE instrument. The first one is the already mentioned large relativistic electrons doses

[32, 41], while the second one is the decrease of the SAA dose rate during the dockings of the USA space shuttle with ISS [64].

Figure 11 shows the result of measurements of the SAA doses for the time span between 22/03/2008 and 01/09/ 2009. SAA proton energies in MeV, maximal dose rates in $\mu\text{Gy h}^{-1}$, and daily dose rates in $\mu\text{Gy d}^{-1}$ are presented in the two panels. The maximal dose rates are the value in the interval from 00:00 to 24:00 h, which is larger than any other SAA 10 s measurement. The largest value here was $1708 \mu\text{Gy h}^{-1}$, and the average was $1218 \mu\text{Gy h}^{-1}$.

The relatively low dose rates at the left side of Fig. 11 have to do with the ISS altitudes in the range of 350—365 km. The increase of the station altitude up to 365—375 km after 21 June 2008 led to an increase of the maximal SAA dose rate above $1200 \mu\text{Gy h}^{-1}$.

The main feature seen in Fig. 11 is that during the five space shuttle docking times the SAA maximal doses fall by $600 \mu\text{Gy h}^{-1}$ and reach an average level of 400—500 $\mu\text{Gy h}^{-1}$ for the STS-123 and STS-124 missions. For STS-126, STS-119, and STS-127, the drop was also $600 \mu\text{Gy h}^{-1}$ from an average level of $1400 \mu\text{Gy h}^{-1}$.

The analysis of the daily average SAA dose rate for the studied period shows that before 21 June 2008 it was around $300 \mu\text{Gy d}^{-1}$, after 21 June 2008 it started to increase, and on 31 July it reached a value of $500 \mu\text{Gy d}^{-1}$, the level at which the daily average SAA dose rate stayed until the end of the observations in September 2009. The dockings of the space shuttles decreased the daily average SAA dose rate by about $200 \mu\text{Gy d}^{-1}$. Similar reductions of the SAA dose rates were observed by Semones (2008) [65] with the TEPC in the Columbus module for the period 4—24 March 2008. Because of the larger shielding inside the Columbus module, the reduction reported in [65] was from 120 to $97 \mu\text{Gy d}^{-1}$ during the STS-123 docking time. Benghin et al. (2008) [66] also reported changes in the ratio of daily dose rates of the unshielded detectors numbers 2 and 3 of the DB-8 system during the shuttle dockings.

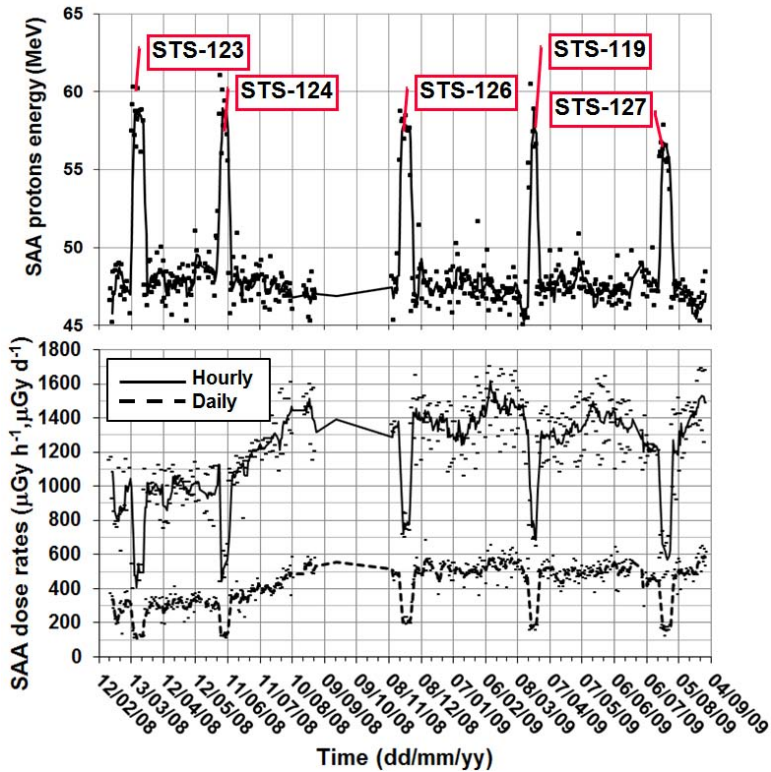


Fig. 11. Daily and hourly SAA dose rates and SAA proton energies measured with the R3DE instrument during the EXPOSE-E mission. The space shuttle dockings at the ISS create strong decreases in the hourly and daily dose rates due to the additional shielding effect of the space shuttle body on the R3DE detector. At the same time the energy of the protons in the SAA increases. The space shuttle visits are marked with the STS number of flight

The investigation of the averaged energy of the protons in the SAA region is shown in the upper panel of Fig. 12, which reveals that the shuttle dockings increased this energy from about 48 MeV to 58 MeV. The energy of the protons incident normally to the detector is calculated by using the experimental formula described by Heffner (1971) [55]. The increase of the averaged proton energy in the SAA region during the shuttle dockings can be explained with the increase of the values in the entire energy range caused by the stopping of the lowest-energy protons in the mass of the space shuttle.

Figure 12 shows the dose rate dynamics observed by 3 different instruments around the time of Space Shuttle (STS-123) docking and

undocking in the time frame 5-31 March 2008. The measured absorbed doses in each exposure interval are presented by black diamonds, while the obtained statistically moving average doses are shown with heavy (red) lines. The numbers there correspond to the number of single measurements used in the moving average calculation.

The 3 panels contain data as follows: In Figure 12a there are the NASA TEPC absorbed dose rate data, which by the selection to be higher than $100 \mu\text{Gy h}^{-1}$ present only the SAA maxima. First part of the data between 5 March and 14:03:37 at 10 March are from position SM-410, while second part till 31 March is from position COL1A3. Data are obtained from <http://cdaweb.gsfc.nasa.gov/> server and prepared by N. Zapp [40]; Figure 12b contains Liulin-5 [45] dose rate data from the first detector selected in same way as the TEPC data; Figure 12c contains R3DE dose rate data selected as the other 2 data sets. Only here the lowest dose rates are $200 \mu\text{Gy h}^{-1}$.

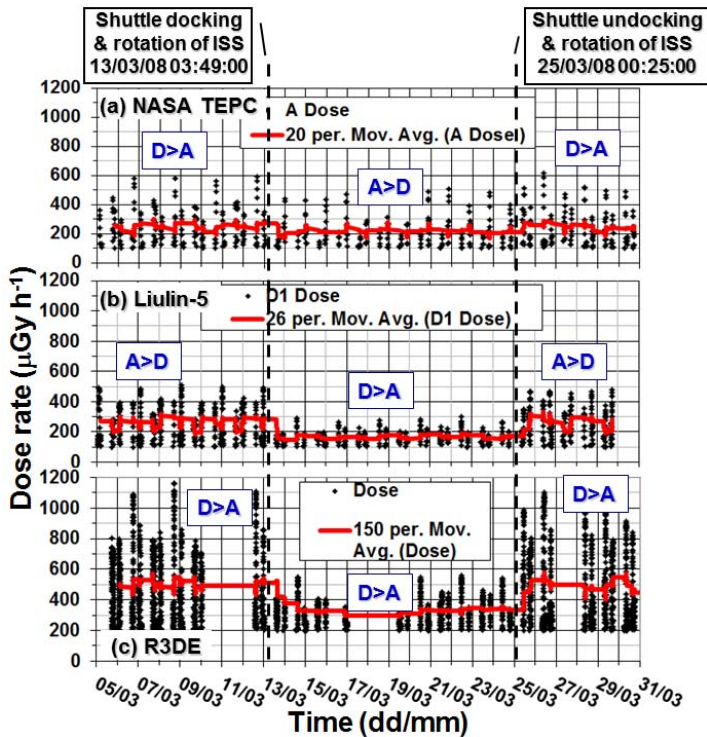


Fig. 12. Variations of the dose rates by NASA TEPC, R3DE and Liulin-5 instruments close to STS-123 docking in the time frame 5-31 March 2008

Because of the large time interval on the X axis in Figure 6 the 6-8 ascending and descending crossings of the SAA anomaly per day are presented by a pair of 2 bars. The first one corresponds to the descending orbits, while the second one to the ascending orbits during one series of 6-8 crossings. The differences in the dose rate amplitudes are produced by the east-west asymmetries of the proton fluxes in the region of the SAA [57]. These amplitudes are additionally stimulated to changes by the attitude of the ISS, which changes by 180° during the Shuttle docking period and reversed after it [67].

The relations between ascending and descending amplitudes of the dose rates for each instruments before, during and after the Shuttle docking are underlined by text boxes, which contain inequalities labelled by $D > A$ when the descending dose rates were greater than ascending ones and in reverse with $A > D$ when the other relation was fulfilled. For the R3DE instrument there were no changes of the amplitudes relations. At any time the descending dose rate value was greater than the ascending one. This behaviour can be explained by the position of the R3DE instrument on the top of EuTEF where it is not shadowed by the Columbus body from SAA protons drifting to the west. The other 2 instruments showed rotation of the ascending descending inequalities connected with the Shuttle docking. These relations are explained more precisely in the next paragraph.

It is well seen that all 3 data sets recorded a decrease in the dose rates after the docking of Space Shuttle at 03:49 on 13th of March 2008. To emphasize the decreases moving averages lines are calculated and presented by heavy lines in each panel of figure 6. For R3DE the decrease in moving averages was from 500 to 300 $\mu\text{Gy h}^{-1}$ or about 40% from the value before the docking. The Liulin-5 data decreased from 300 to 180 $\mu\text{Gy h}^{-1}$ or again about 40% from the value before the docking. TEPC dose rates obtain the smallest decrease from 280 to about 200 $\mu\text{Gy h}^{-1}$, which is about 30% decrease. Dose rates measured by all 3 instruments returned to the values before the docking of STS-123 after 00:25 on 25th of March, when the undocking of Space Shuttle occurred.

3.2.6. R3DR instrument results

The R3DR spectrometer (see Table 1, Item No 11) was launched inside of the EXPOSE-R facility to the ISS in December 2008 and was mounted at the outside platform of the Russian Zvezda module of the ISS.

The first data were received on March 11, 2009. Until the end of August 2010 the instrument worked almost continuously with 10 seconds resolution; the data were recorded on the ISS. Comprehensive presentation of the R3DR results inside of the EXPOSE-R facility can be found in [68].

In Figure 4 there was already presented a comparison of data obtained simultaneously by R3DE/R instruments and NASA TEPC. The main conclusion from the comparisons of data between R3DE and R3DR instruments [41] is that the values of the dose rates produced by different radiation sources around the ISS did have large and rapid variations in space and time. All obtained data can be interpreted as possible doses obtained by cosmonauts and astronauts during Extra Vehicular Activities (EVA) because the R3DE/R instrument shielding is very similar to the Russian and American space suits' average shielding [3]. Fast, active measurements at the body of each astronaut to obtain the exact dynamics of the dose accumulation during EVA are required.

An instrumental solution was proposed in [69], where the possible hardware and software improvements for a new Liulin type dosimeter were proposed. New instruments will be able, on the basis of the analysis of the shape of the deposited energy spectrum and the value of the dose to flux ratio, to distinguish the different types of radiation sources in the ISS radiation environment as GCR, IRB protons and outer radiation belt electrons. They will measure, calculate, store and present on display the fast variations of the absorbed and ambient dose equivalent doses in any of the possible surrounding mass distributions.

3.3. Experiments and results on satellites

3.3.1. Results obtained at Foton M2/M3 satellites

Radiation Risks Radiometer-Dosimeter (R3D) for Biopan (R3D-B) with 256 channels ionizing radiation monitoring spectrometer and four channels UV spectrometer known as R3D-B2 (see Table 1, Item No 3) was successfully flown 31 May–16 June 2005 inside of the ESA Biopan 5 facilities on Foton M2 satellite. The operation time of the instrument was about 20 days for fulfilling of the total 1.0 MB flash memory with 30 s resolution [70]. R3D-B3 spectrometer (see Table 1, Item No 7) was with almost same mechanical characteristics as R3D-B2. Larger 2.0 MB flash memory was used for about 30 days measurements. It was successfully flown 14–29 September 2007 inside of the ESA Biopan 6 facilities on Foton

M3 satellite. Together with R3D-B3, the Liulin-Photo instrument (see Table 1, Item No 8) was flown but inside of the capsule of the Foton M3 satellite [70a]. Most important findings in the R3D-B2/B3 data were the measurements of high doses delivered by relativistic electrons at altitudes below 300 km and latitudes above 50° geographic latitude in both hemispheres [7].

3.3.2. Results obtained at Chandrayaan satellite

RADOM spectrometer-dosimeter (see Table 1, Item No 10) was successfully used on the Indian Chandrayaan-1 Moon satellite from 22 October 2008-30 August 2009. It started working 2 h after the launch with 10 seconds resolution behind about 0.45 g cm⁻² shielding. The instrument sent data for a number of crossings of the Earth radiation belts and continued to work on 100 and 200 km circular lunar orbits measuring mainly the GCR environment [34].

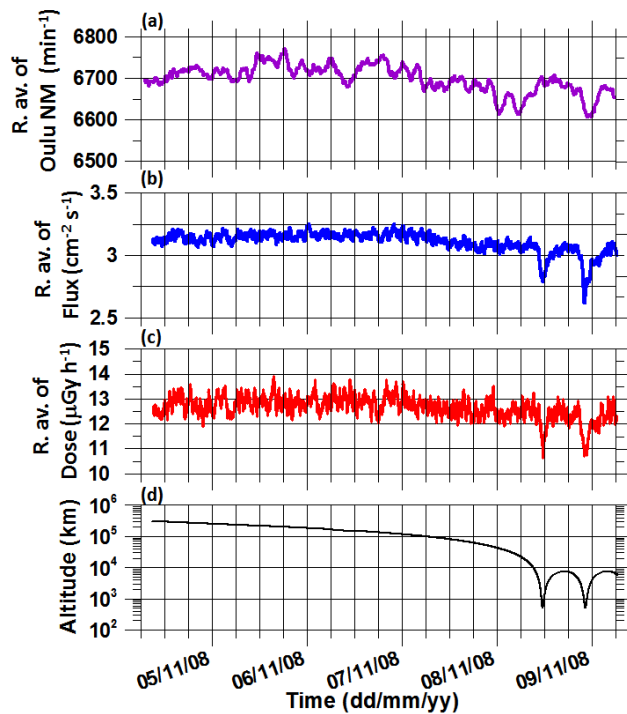


Fig. 13. RADOM observations during lunar transfer trajectory and lunar orbit capture. The distance is from the Moon. The trends in particle flux coincide with the Oulu neutron monitor data trends

Chandrayaan-1 was placed into the lunar transfer trajectory on 3rd November 2008 (13th day after launch) and a lunar orbit capture manoeuvre was carried out on 8th November (18th day after the launch). Fig. 13 shows RADOM observations for about 3 days before the lunar orbit capture and about one day after it. More than 40000 measurements with 10 s resolution are used for the figure. Figures 13b and 13c show the moving average over 200 points of measured particle flux and the absorbed dose rate respectively. Figure 13d shows the distance from the Moon (in km), while the Figure 9a shows the Oulu Neutron Monitor running average of measured count rate per minute averaged over 10 minutes. The average dose rate from more than 33000 measurements in the altitudinal range between 308000-20000 km from the Moon is $\sim 12.76 \mu\text{Gy h}^{-1}$. The range of the real measured dose rates is between 3.34 and 41.34 $\mu\text{Gy h}^{-1}$ with a standard deviation of 4.25 $\mu\text{Gy h}^{-1}$. The average flux is 3.14 particles $\text{cm}^{-2} \text{cm}^{-2} \text{s}^{-1}$, while the real flux range is between 1.71 and 4.82 particles $\text{cm}^{-2} \text{s}^{-1}$ with a standard deviation of 0.41 $\text{cm}^{-2} \text{s}^{-1}$. Figures 13b and 13c don't show this real dynamics of the values because the moving averages are plotted there. These values of the dose rate and flux may be used as referee values for the "deep space" radiation conditions at this very low level of solar activity and respectively.

For the above mentioned altitudinal range the flux correlates with the Oulu NM count rate and respectively with the solar activity. Later on during the two closer approaches to the Moon at an altitude about 508 km the flux and the dose rate decrease because the enhanced shielding of the cosmic rays by the Moon body itself. A closer look at the Figure 13a reveals that the second periselene crossing is deeper than the first one. This is mostly related with a local increase of the solar activity as evident from the simultaneous decrease of the Oulu NM count rate.

RADOM observations which began within two hours after launch of the Chandrayaan-1 and continued until the end of the mission demonstrated that it could successfully characterize different radiation fields in the Earth and Moon environments. Signature and intensity of proton and electron radiation belts, relativistic electrons in the Earth magnetosphere as well as galactic cosmic rays were well recognized and measured. Effect of solar modulation of galactic cosmic rays could also be discerned in the data. The electron radiation belt doses reached $\sim 40000 \mu\text{Gy h}^{-1}$, while the maximum flux recorded was $\sim 15000 \text{cm}^{-2} \text{s}^{-1}$. The proton radiation belt doses reached the highest values of $\sim 130000 \mu\text{Gy h}^{-1}$, while the maximum flux was $\sim 9600 \text{particle cm}^{-2} \text{s}^{-1}$. Comparison of these results with other similar instruments

on board ISS shows good consistency, indicating nominal performance RADOM. Outside the radiation belts, en-route to the Moon, the particle flux (~ 3 particle $\text{cm}^{-2} \text{s}^{-1}$) and corresponding dose were very small ($\sim 12 \mu\text{Gy h}^{-1}$) which further decreased slightly in the lunar orbit because of the shielding effect of the Moon. Average flux and dose in lunar orbit were $\sim 2.45 \text{ cm}^{-2} \text{ s}^{-1}$, and the corresponding absorbed dose rate was $9.46 \text{ cm}^{-2} \text{ s}^{-1}$ respectively at 100 km orbit. These increased to 2.73 particles $\text{cm}^{-2} \text{ s}^{-1}$ and $10.7 \mu\text{Gy h}^{-1}$ respectively, at 200 km orbit. The total accumulated dose during the transfer from Earth to Moon was found to ~ 1.3 Gy.

3.3.3. Results obtained at “BION-M” №1 spacecraft

“BION-M” №1 was a low Earth orbit satellite that orbited the Earth with a period of 89.9 min, an inclination of 65° with respect to the Earth’s equator, and with an altitude above the Earth surface in the range 253–585 km. The final orbit of the satellite was almost circular with an apogee of 585 km and a perigee of 555 km altitude. The final orbital parameters were reached after 21 April 2013 [71]. Space radiation has been monitored using the RD3-B3 spectrometer-dosimeter (see Table 1, Item No 13), which was mounted inside of the satellite in a pressurized volume together with biological objects and samples. The RD3-B3 instrument is a battery operated version of the spare model of the R3D-B3 instrument developed and built for the ESA BIOPAN-6 facility on Foton M3 satellite in September 2007 [70].

The observed hourly and daily IRB dose rates at the “BION-M” №1 satellite are the highest seen by us during our measurements on “Mir” and the ISS space station and on Foton-M2/M3 satellites because the altitude of the “BION-M” №1 orbit was the highest in comparison with all missions mentioned above. The same is valid for the GCR doses. The observed ORB doses are smaller than the ones measured outside the ISS because of the higher shielding on the “BION-M” №1 satellite.

3.4. Main experiments and results at aircraft balloon and rocket

Table 2 lists DES Liulin type experiments on aircraft, balloon, rocket and mountains peaks. The pictures shown for items 2 and 8 are the latest versions of the instruments used in this category. For some of the mentioned in these rows references the instruments was housed in different that the shown in the pictures.

The Liulin-4C, MDU#2 instrument (see Table 2, Item No 1) worked successfully during the flight of French balloon up to 32 km altitude in the region of the Gap town in Southern France on 14th of June 2000. This experiment was performed by the Nuclear Physics Institute, Czech Academy of Sciences [72].

One battery-powered DES of Liulin-4J (see Table 2, Item No 1) type performed dosimetric measurements of the ionizing radiation environment at ~20 km altitude aboard NASA's Lockheed ER-2 high altitude research aircraft in October-November 2000 from Edwards Air Force Base (AFB) in Southern California and flew over the border region dividing Central California from Central Nevada [73].

Mobile Dosimetry Units MDU-5 and 6 (see Table 2, Item No 2) was used for long-term measurements between 2001 and 2014 on Czech Airlines (CSA) aircraft at different routes. Data obtained were used for comparison with model calculated doses for the purposes of individual monitoring of aircrew [30, 31]. Fig. 14 presents almost one solar cycle data from these flights, which are publicly available in database of measurements. (<http://hroch.ujf.cas.cz/~aircraft/>) [74, 74a]. Please see Fig. 14 captions for more details.

Very similar instruments to the Mobile Dosimetry Units MDU-5 and 6 was used by scientific groups in Spain [76] and Korea [77] for radiation measurements at aircrafts.

Three battery-powered DES (see Table 2, Item No 3) were operated during the 8 June 2005 certification flight of the NASA Deep Space Test Bed (DSTB) balloon at Ft. Sumner, New Mexico, USA. The duration of the flight was about 10 hours (http://wrmiss.org/workshops/tenth/pdf/08_benton.pdf).

Liulin-6S, Lilun-M, Liulin-6MB and Liulin-6R (see Table 2, Item No 4) are internet based instruments [78]. They use internet module to generate web page. The obtained deposited energy spectra data are transmitted via LAN interface by HTTP and FTP protocols. They worked for different periods since 2005 at Jungfrau (Switzerland) 3453 meters Above Mean Sea Level (AMSL) <http://130.92.231.184/>, Moussala (Bulgaria) 2925 meters AMSL <http://beo-db.inrne.bas.bg/moussala/> and Lomnický štít (Slovakia) 2633 meters AMSL <http://147.213.218.13/> peaks and at ALOMAR observatory in Norway (<http://128.39.135.6/>) [17]. The three peak instruments are working well till now (April 2014) and their data can be obtained online on the mentioned above addresses.

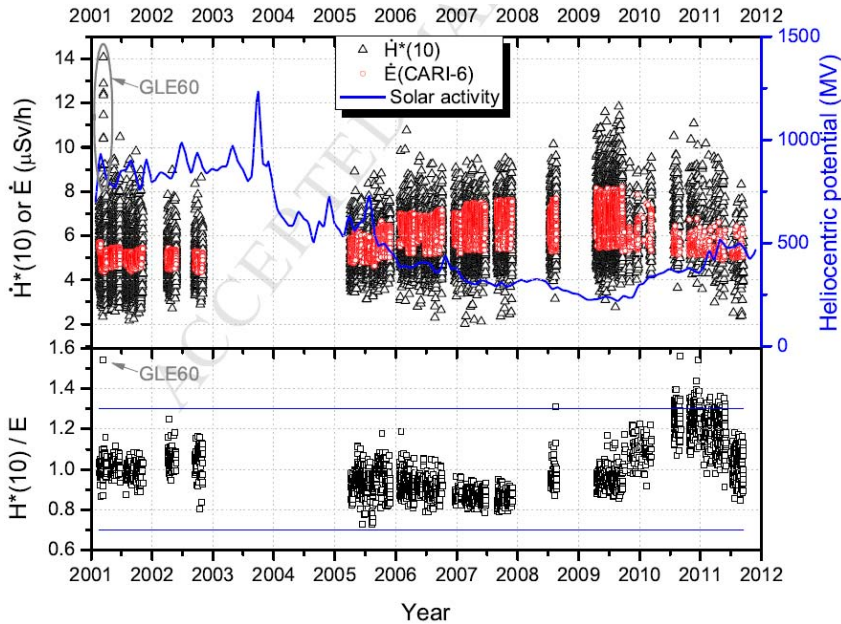


Fig. 14. Top panel: Ambient dose equivalent ($H^*(10)$ - black triangle) dose rates determined by Liulin and effective dose rates ($E(\text{Cari-6})$ – red circles) calculated with CARI-6 code [75] plotted as a function of time (only data at 35000 (10.67 km) and effective vertical cut-off rigidity [14] ($VCR \leq 3.5$ GV) are shown).

Solar activity is expressed via the heliocentric potential).

Bottom panel: Ratios of integral values per whole flight between ambient dose equivalents, $H^*(10)$, estimated with Liulin, and effective doses, E , calculated with CARI-6 plotted as a function of time. $\pm 30\%$ confidence band is plotted with 2 horizontal blue lines

Liulin-4SA (see Table 2, Item No 5) spectrometer was designed in 2005 under the request of Captain Ian Getley pilot of Boeing 747-400, Qantas Airways aircraft [44]. Liulin-4SA was used inside of the cockpit of Boeing 747-400 aircraft and provided on LCD display data for the local dose rate and flux simultaneously with the flight altitude, longitude and latitude, obtained from build-in GPS receiver for each measurements interval (usually 60 sec). Pre-programmed alert signals was able to be initiated when the measured dose rate exceed preliminary set levels for 3 subsequent measurement intervals.

The presented in Table 2, Item No 6 two Liulin DES systems consists of 4 dosimetry units (DU) and 1 control and interface unit (CIU).

The Liulin-6U instrument was delivered to NASA, Marshall Space Flight Center, USA in 2005. It was planned to be used in a balloon experiment [79]. The second one is delivered to the Skobeltsyn Institute of Nuclear Physics at Lomonosov Moscow State University in 2010. It was planned to be used in the RAZREZ system for RADIOSCAF experiment on ISS [80, 81].

Liulin-R instrument (see Table 2, Item No 7) was successfully launched on HotPay2 rocket from Andoya Rocket Range (ARR), Norway, on 31st of January, 2008 at 19:14:00 and rising up to 380 km altitude, as a part of an EU financed scientific program called eARI (ALOMAR eARI project) [82].

Wissmann et al. [83] performed 5 balloon experiments up to 30 km altitude using Liulin-6RG spectrometers (see Table 2, Item No 8) between July 2011 and August 2012. The Liulin instruments were powered and transmitted the obtained in 30 sec deposited energy spectrum to data logger, developed in Physikalisch-Technische Bundesanstalt (PTB), Germany.

The presented in Table 2, Item No 9 Liulin spectrometer is the last generation of series of instruments with build-in GPS receiver and 1 or 2 MB SD card. First this type of instruments (LIULIN-4N) was used by colleagues from Department of Chemistry and Chemical Engineering, Royal Military College of Canada in 2003-2005 [43, 84]. Two different methods of determining the route $H^*(10)$ value from the LIULIN data were examined, which agree very well the $H^*(10)$ values measured by the TEPC (within the 20% error inherent within both instruments).

3.5. Profile of the ionizing radiation exposure between the Earth surface and free space

Fig. 15 presents the synthesized altitudinal profiles of the moving averages (over 4 points) of 3 parameters: absorbed dose rate in $\mu\text{Gy h}^{-1}$ (heavy line), flux in $\text{cm}^{-2} \text{s}^{-1}$ (long (red) dashed line) and specific dose (SD) in $\text{nGy cm}^2 \text{particle}^{-1}$ (short (blue) dashed line). On the left side of the figure are listed the carriers, instruments, time, averaged geographic coordinates of the measured values and their altitudinal range in km. On the right side are listed the conditions and predominant radiation sources for the places pointed with the arrows. The figure is similar to the published in [86] Fig.2 but improved with the new data obtained with RD3-R3 instrument on

“BION-M” No1 satellite and Liulin-5 data on ISS for the period of flight of “BION-M” No1 satellite - 21/04/-13/05/2013.

Fig. 15 contains original experimental data, which are compared and plotted to reveal a unified picture how the different ionizing radiation sources contribute and build the space radiation exposure altitudinal profile from the Earth surface up to the free space. The dose rate and flux data cover 7 orders of magnitude and can be used for educational purposes and also as reference values for new models. The presentation of data in kilometers above the Earth surface instead in L values allows space agencies medical staff and that not specialized in the geophysics support to use them for a first approach for the expected human exposure at different altitudes and also the general public and students to have a simple knowledge about the position of the most common maxima of exposure around the Earth and up to free space.

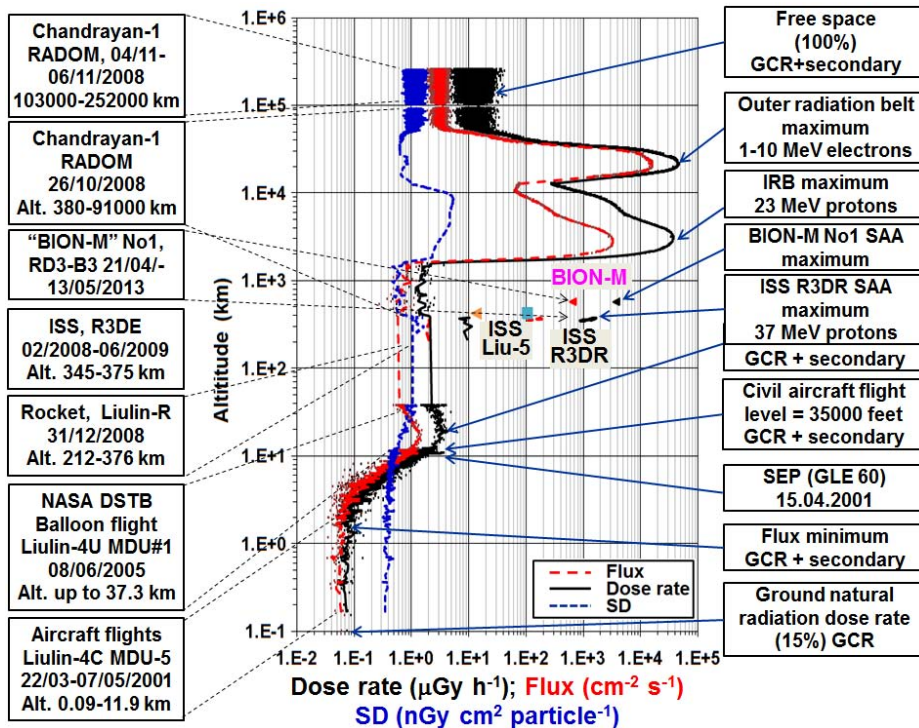


Fig. 15. Variations of the absorbed dose rate, flux and specific dose for altitudinal range from 0.1 to 250,000 km. (For interpretation of the references to color in this figure legend, the reader is referred to the web version of this article.)







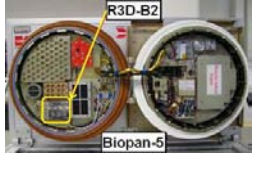



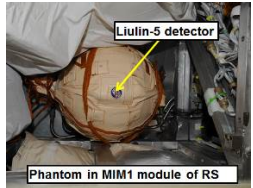

Conclusions

The Liulin type low mass, dimension and price instruments during the period 1989-2014 proved their ability to characterize the radiation environment at the: ground, mountain peaks, aircraft, balloon, rocket and spacecraft.

Acknowledgements

The authors would like to thank to: V. Petrov, V. Shurshakov, V. Benghin and I. Chernykh from Institute of Biomedical Problems, Moscow, Russia for the long lasting and fruitful scientific cooperation since the development of the first LIULIN instrument in 1986; G. Horneck and G. Reitz from DLR, Institute of Aerospace Medicine, Germany, D.-P. Häder, M. Lebert and M. Schuster from Department für Biology der Friedrich-Alexander-Universität, Germany for the leadership and cooperation in the experiments on ESA Foton-M2/M3 spacecraft and ISS; F. Spurny, and O. Ploc from Nuclear Physics Institute, Czech Republic for work on the radiological interpretation of Liulin data and for the leadership in the use of Liulin instruments on aircraft; K. Fujitaka, Y. Uchihori and H. Kitamura from National Institute of Radiological Sciences, Chiba, Japan for the leadership in the calibrations of Liulin instruments on protons and heavy ions; J. Lemaire, from Institut d'Aeronomie Spatiale de Belgique for the help in the interpretation of LIULIN data; Gh. Gregoire and H. Schnitz from Institut de Physique, Universite Catholique de Louvaln, Belgique, for the Liulin-ISS calibrations; E.G. Stassinopoulos, former Director of NASA-GSFC Radiation Physics Office for the support and help in the Liulin-3M calibrations; E. Benton from Department of Physics, Oklahoma State University, USA for the support and NASA balloon data; J. Miller, Lawrence Berkeley National Laboratory, Berkeley, USA for the post-calibrations of LIULIN instrument; ISRO staff and more specially to: M. Annadurai, Project Director and J.N. Goswami, Project scientist of Chandrayaan-1 satellite, P. Sreekumar and V. Sharan, Space Astronomy & Instrument Division, ISRO, Bangalore, India for the RADOM instrument support; M.T. Giardi and M. Damasso, Institute of Crystallography-National Research Council, Roma, Italy for the Liulin-Photo cooperation.

Table 1. Liulin type experiments performed during satellite missions

Item No	Satellite Date begin-Date end Available number of measurements	Experiment name PI CoPI References	Instrument Size [mm]/Mass [kg] Place Shielding [g cm ⁻²] Resolution [sec]/[min]	Instrument Location image	External view of the instrument
1	MIR SS 04/1988-06/1994 > >2,000,000 measurements	LIULIN V. Petrov, IMBP; Ts. Dachev, SRTL. Dachev, et al., 1989. [17]; Shurshakov et al., 1999. [54].	LIULIN 1 DU (109x149x40 mm, 0.45 kg); 1 MCU (300x220x187 mm, 6.5 kg) Inside different modules of MIR SS >5 g cm ⁻² 30 sec		
2	Mars-96 16/11/1996 (The satellite was lost because of rocket booster malfunctioning)	RADIUS-MD V. Petrov, IMBP; Ts. Dachev, SRTL. Semkova et al., 1994. [18].	2 Solid State Detectors (SSD) (154x80x70 mm, 0.38 kg) Outside and inside Mars-96 satellite > >2 g cm ⁻² ; 10 min		
3	ISS 05/05/2001- 26/08/2001/ 1,267,200	Dosimetric Mapping G. Reitz, DLR; Ts. Dachev, SRTL. Dachev et al., 2002. [20]; Reitz et al., 2005. [10]; Nealy et al., 2007. [58]; Slaba et al., 2011. [59].	Liulin-E094 1 CIU (120x80x60 mm, 0.4 kg) 4 MDU (100x64x24 mm, 0.23 kg) Inside of the American Lab. and Node 1 of ISS > >20 g cm ⁻² ; 30 sec		
4	Foton M2 01/06/2005- 12/06/2005 17,280	Biopan 5 G. Horneck, DLR; D. Häder, UE; Ts. Dachev, SRTL. Häder et al., 2009. [70]; Dachev et al., 2009. [7].	R3D-B2 (57x82x24 mm, 0.12 kg) 1 DU outside of the satellite and inside of Biopan-5 facility 1.75 g cm ⁻² ; 60 sec		
5	ISS Since Sept. 2005 13/08/2008- 29/08/2008 Service system in next 15 years 149,760 spectra	Liulin-ISS V. Petrov, IMBP; Ts. Dachev, SRTL. Dachev, et al., 2005. [60].	Liulin-MKS 1 CIU (120x80x20 mm, 0.4 kg) 4 MDU (110x80x25 mm, 0.23 kg) Inside Russian segment of ISS >20 g cm ⁻² ; 10-3599 sec		
6	ISS 17/05/2007- Working permanently against flash memory card >2,500,000 measurements	Matroska-R V. Petrov, IMBP; J. Semkova, SRTL. Semkova, et al., 2003. [21]; Semkova, et al., 2008. [22].	Liulin-5, Dosimetric telescope by 3 detectors (50/30x191 mm, 0.4 kg) Electronic block (160x90x30 mm, 0.8 kg) Inside Russian segment of ISS >20 [g cm ⁻²]; 90 sec		

7	Foton M3 14/09/2007- 26/09/2007 18,720	Biopan 6 G. Horneck, DLR; D. Häder, UE; Ts. Dachev, SRTL. Damasso et al., 2009. [70a]; Häder et al., 2009. [70].	R3D-B3 1 DU (57x82x24 mm, 0.12 kg) outside of the satellite and inside of Biopan-6 facility 0.8 g cm ⁻² ; 60 sec		
8	Foton M3 14/09/2007- 26/09/2007 27,360	PHOTO-II M.-T. Giardy, IC- AR, Rome, Italy; Ts. Dachev, SRTL. Damasso et al., 2009. [70a].	Liulin-Photo, 1 DU (57x82x24 mm, 0.5 kg) Above Photo instrument, inside of the satellite, > >5.0 g cm ⁻² ; 60 sec		
9	ISS, Columbus module 17/02/2008- 03/09/2009 4,406,400	EXPOSE-E G. Horneck, DLR; D. Häder, UE; Ts. Dachev, SRTL. Häder and Dachev, 2003. [70] Dachev et al., 2012. [32]	R3DE 1 DU (76x76x36 mm, 0.19 kg) Outside of ISS in EXPOSE-E facility in EuTEF > >0.6 g cm ⁻² ; 10 sec		
10	Chandrayaan-1 satellite around the Moon 22/10/2008- 29/09/2009 1,209,600 spectra	RADOM Ts. Dachev, SRTL Dachev et al., 2011. [34]; Dachev, 2013. [85].	RADOM 1 DU (110x40x20 mm, 0.098 kg) Outside of the Chandrayaan-1 satellite > >0.6 g cm ⁻² ; 10 and 30 sec		
11	ISS, Zvezda module 11/03/2009- 20/08/2010 3,540,000	EXPOSE-R G. Horneck, DLR; D. Häder, UE; Ts. Dachev, SRTL. Dachev et al., 2013. [8] Dachev 2013. Dachev et al., 2014	R3DR 1 DU (76x76x36 mm, 0.19 kg) Outside of ISS in EXPOSE-E facility outside of Zvezda module > >0.6 g cm ⁻² ; 10 sec		
12	Phobos-Grunt 09/11/2011 (The satellite was lost because of rocket booster malfunctioning)	Liulin-Phobos V. Petrov, IMBP; J. Semkova, SRTL. Semkova, et al., 2008. [22].	Liulin-Phobos 2x2 dosimetric telescopes (172x114x45 mm 0.5 kg) Outside Phobos-Grunt satellite; >2 g cm ⁻² Dose and flux 60 sec Spectrum 60 min		

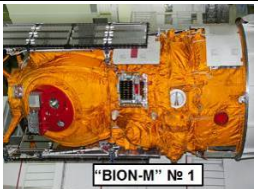
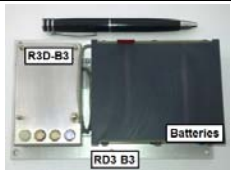









13	<p>"BION-M" №1 19/04/2013- 1305.2013</p> <p>In space 34, 391 spectra</p>	<p>RD3-B3</p> <p>V. Shurshakov, IMBP; Ts. Dachev, SRTI</p> <p>Dachev et al., 2014. [71].</p>	<p>RD3-B3 (110x80x44 mm, 0.3 kg)</p> <p>1 battery operated DU Inside "BION-M" №1 satellite/ ></p> <p>>2 [g cm⁻²]; 60 sec</p>		
----	--	--	---	---	--

Table 2. Liulin type experiments at aircraft, balloon, rocket and mountains peaks

Item No	Experiment description Date begin-Date end	Person performing the experiment References	Instrument Size [mm]/Mass [kg] Place Resolution [sec]	External view of the instrument
1	<p>1. Balloon experiment at Gap-Tallard aerodrome, France, 14/06/2000;</p> <p>2. NASA's Lockheed ER-2 high altitude research aircraft, Oct.-Nov. 2000.</p>	<p>1. CNES balloon technological flight program, F. Spurny, NPI-CAS, Prague, Czech Republic;</p> <p>2. Y. Uchihori, NIRS, Japan;</p> <p>Spurny, F., 2000. [72]. Uchihori et al., 2003. [73].</p>	<p>Liulin-4C/4J, MDU-2 (100x64x24 mm, 0.23 kg with rechargeable Li-Ion battery pack)</p> <p>Inside of the balloon gondola or the ER-2 cockpit, 60 sec.</p>	
2	<p>Long-term (>60 days) measurements at aircraft altitudes for different airlines. 28 V DC/DC converter.</p> <p>Since 2001 up to 2014.</p>	<p>F. Spurny and O. Ploc, NPI, Czech Rep; Ploc et al., 2013. [74]</p> <p>J.C. Saez Vergara and R. Dominguez-Mompell Roman, CIEMAT and IBERIA, Spain [76].</p> <p>Hwang et al, KASI, Korea [77]</p>	<p>DU (110x100x45 mm, 0.48 kg including 2 D size Lithium-Ion batteries)</p> <p>Inside of the aircraft</p> <p>300/600 sec.</p>	
3	<p>Deep Space Test Bed (DSTB) certification flight</p> <p>8 June 2005 at Ft. Sumner, New Mexico, USA. ~10 hours</p>	<p>E. R. Benton, ERIL Research Inc.</p> <p>Benton, 2005. http://wrmiss.org/workshops/tenth/pdf/08_benton.pdf</p>	<p>3 Liulin MDU (100x64x24 mm, 0.23 kg with rechargeable Li-Ion battery pack)</p> <p>Inside of the balloon gondola 60 sec.</p>	
4	<p>Measurements at mountain peaks. The Liulin instrument contains Internet module to post, store and transmit the obtained results via FTP protocol in Internet.</p>	<p>Bern university, Jungfrau, Switzerland: http://130.92.231.184/</p> <p>Lomnitski Shtit: http://147.213.218.13/</p> <p>INRNE-BAS, BEO-Moussala: http://beo-db.inrne.bas.bg/moussala/</p>	<p>DU (84x40x40 mm, 0.12 kg.</p> <p>Internet module with 22 MHz microprocessor, 512K flash and 512K SRAM memory. 600 sec.</p>	
5	<p>Measurements at aircraft altitudes. A built in GPS receiver record: UT, Longitude, Latitude and Altitude, which together with the dose rate data are shown on the display.</p>	<p>I. Getley, University of New South Wales, Australia</p> <p>Getley et al., 2010. [44].</p>	<p>Spectrometer (110x55x45 mm; 0.38 kg); Display (115x40x20 mm; weight 0.12 kg); Rechargeable battery package (90x60x40 mm; 0.18 kg). Inside of the cockpit of Boeing 747-400 Qantas Airways flights. 60 sec.</p>	

6	1. NASA balloon experiment for radiation studies. 2. RAZREZ system on ISS (The both systems are already delivered but both exp. are not performed.)	1. J. Adams et al., 2007. [79]. NASA/Marshall Space Flight Center, USA. 2. Petrov et al., 2009. [80] http://wrmiss.org/workshops/fourteenth/Petrov.pdf	4 DU (74x40x20 mm, 0.065 kg; 1 CIU (144x60x20 mm, 0.21 kg) Total 0.47 kg. Powered from 28 V DC, 0.72 mA. Data transmission trough RS485 interface.	
7	Under the HotPay2 project from Andoya Rocket Range, Norway was launched a rocket up to 380 km altitude on January 31, 2008.	Tomov et al., 2009. [82]. http://www.stil.bas.bg/FSR/PDF/TOP5_Tomov_Borislav2242058.pdf	(110x40x20 mm, 0.098 kg) Inside of the rocket payload 60 sec.	
8	5 balloon flights up to 30 km altitude between July 2011 and August 2012	F.Wissmann et al., Physikalisch-Technische Bundesanstalt (PTB), Germany F.Wissmann et al., 2013. [83]	Liulin-RG4/5 2 DU (110x40x20 mm 0.092 kg). With serial readout of the data measured with the Si-detector. On the gondola of the balloon. 30 sec.	
9	Long-term (>60 days) measurements at aircraft altitudes. A built in GPS receiver record: UT, Longitude, Latitude and Altitude. Data are stored at 1 or 2 GB SD card. 28 V DC/DC converter. Since 2005 up to 2014.	A.R. Green et al., Royal Military College of Canada, Canada. Green et al., 2005. [43]; Kitching, 2004. [84].	1 DU (110x100x45 mm, 0.48 kg including 2 D size Lithium-Ion batteries) inside of the aircraft 300/600 sec	

References

1. Badhwar, G.D., W. Atwell, B. Cash, V.M. Petrov, Yu.A. Akatov, I.V. Tchernykh, V.A. Shurshakov, V.A. Arkhangelsky, Radiation environment on the MIR orbital station during solar minimum. *Adv. Space. Res.* 22 (4), 1998, 501-510.
2. Benton, E.R., E.V. Benton, Space radiation dosimetry in low-Earth orbit and beyond, *Nucl. Instrum. and Methods in Physics Research, B*, 184, (1-2), 2001, 255-294.
3. Benton, E.R., E.V. Benton, A.L. Frank, M.F. Moyers, Characterization of the radiation shielding properties of US and Russian EVA suits using passive detectors, *Radiation Measurements*, 41, 2006, 1191-1201.
4. NCRP, Report No. 142, Operational Radiation Safety Program for Astronauts in Low-Earth Orbit: A Basic Framework - Report No. 142, Bethesda, MD, 2002.
5. Simpson, J.A., Composition and origin of cosmic rays. In: Shapiro, M.M. (Ed.), *NATO ASI Series, Series C Mathematical and Physical Sciences*, 1983, 107. Reidel, Dordrecht.

6. Kim, M.-H.Y., G., De Angelis, F.A. Cucinotta, Probabilistic assessment of radiation risk for astronauts in space missions. *Acta Astronautica* 68 (7–8), 2010, 747–759.
7. Dachev, Ts.P., B.T. Tomov, Yu.N. Matviichuk, P.G. Dimitrov, N.G. Bankov, Relativistic electrons high doses at international space station and Foton M2/M3 satellites. *Advances in Space Research* 44, 2009, 1433–1440. <http://dx.doi.org/10.1016/j.asr.2009.09.023>.
8. Dachev Ts.P., B.T. Tomov, Yu.N. Matviichuk, Pl.G. Dimitrov, N.G. Bankov, G. Reitz, G. Horneck, D.-P. Häder, M. Lebert, M. Schuster, Relativistic Electron Fluxes and Dose Rate Variations during April-May 2010 Geomagnetic Disturbances in the R3DR Data on ISS, *Adv. Space Res.* 50, 2012, 282-292. <http://dx.doi.org/10.1016/j.asr.2012.03.028>.
9. Dachev Ts.P., B.T. Tomov, Yu.N. Matviichuk, Pl.G. Dimitrov, N.G. Bankov, G. Reitz, G. Horneck, D.-P. Häder, M. Lebert, M. Schuster, Relativistic Electron Fluxes and Dose Rate Variations Observed on the International Space Station. *J. Atmospheric and Solar-Terrestrial Physics*, 99, 2013, 150-156. <http://dx.doi.org/10.1016/j.jastp.2012.07.007>.
10. Reitz G., R. Beaujean, E. Benton, S. Burmeister, Ts. Dachev, S. Deme, M. Luszik-Bhadra, and P. Olko, Space radiation measurements on-board ISS—the DOSMAP experiment. *Radiat Prot Dosimetry*. 116, 2005, 374-379. <http://rpd.oxfordjournals.org/cgi/content/abstract/116/1-4/374>.
11. Mertens, C.J., J.W. Wilson, S.R. Blattinig, S.C. Solomon, M.J. Wiltberger, J. Kunches, B.T. Kress, J.J. Murray, Space weather nowcasting of atmospheric ionizing radiation for aviation safety, NASA Langley Research Center, 2007. Available online at: http://ntrs.nasa.gov/archive/nasa/casi.ntrs.nasa.gov/20070005803_2007005368.pdf
12. Lantos, P., The Sun and its effects on the terrestrial environment. *Radiation Protection Dosimetry* 48 (1), 1993, 27–32.
13. Bazilevskaya, G.A., Y.I. Stozhkov, A.K. Svirzhevskaya, N.S. Svirzhevsky, Cosmic rays and radioactivity in the near-ground level of the atmosphere. *Journal of Physics* 409, 2013, 012213. <http://dx.doi.org/10.1088/1742-6596/409/1/012213>.
14. Shea M.A., D.F. Smart, Vertical cutoff rigidities for cosmic ray stations since 1955. In: 27th International Cosmic Ray Conference. *Contributed Papers*, 10, 2001, 4063–4066.
15. Wilson, J.W., D.L. Maiden, P. Goldhagen, H. Tai, J.L. Shinn, Overview of Atmospheric Ionizing Radiation (AIR). NASA Langley Research Center, 2003. Available online at: http://ntrs.nasa.gov/archive/nasa/casi.ntrs.nasa.gov/20030063010_2003072785.pdf
16. Wahl, L.E., Environmental Radiation, 2010. Available online at: http://hps.org/documents/environmental_radiation_fact_sheet.pdf, Fig 1., reprinted from <http://www.ncrppublications.org/Reports/160>).

17. Dachev, Ts.P., Yu.N. Matviichuk, J.V. Semkova, R.T. Koleva, B. Boichev, P. Baynov, N.A. Kanchev, P. Lakov, Ya.J. Ivanov, P.T. Tomov, V.M. Petrov, V.I. Redko, V.I. Kojarinov, R. Tykva, Space radiation dosimetry with active detections for the scientific program of the second bulgarian cosmonaut on board the Mir space station, *Adv. Space Res.*, 9, 10, 1989, 247-251. [http://dx.doi.org/10.1016/0273-1177\(89\)90445-6](http://dx.doi.org/10.1016/0273-1177(89)90445-6).
18. Semkova, J., Ts. Dachev, Yu. Matviichuk, R. Koleva, B. Tomov, P. Bajnov, V. Petrov, V. Nguyen, M. Siegrist, J. Chene, C. d'Uston, F. Cotin, Dosimetric investigation on MARS-96 missions, *Adv. Space Res.*, V 14, No.10, 1994, 707-710. [http://dx.doi.org/10.1016/0273-1177\(94\)90530-4](http://dx.doi.org/10.1016/0273-1177(94)90530-4).
19. Dachev, Ts.P., E.G. Stassinopoulos, B.T. Tomov, Pl.G. Dimitrov, Yu.N. Matviichuk, V.A. Shurshakov, V.M. Petrov, Analysis of the Cyclotron Facility Calibration and Aircraft Results Obtained by LIULIN-3M Instrument, *Adv. Space Res.*, 32, 2003, 67-71. doi:10.1016/S0273-1177(03)90372-3.
20. Dachev Ts., B. Tomov, Yu. Matviichuk, Pl. Dimitrov, J. Lemaire, Gh. Gregoire, M. Cyamukungu, H. Schmitz, K. Fujitaka, Y. Uchihori, H. Kitamura, G. Reitz, R. Beaujean, V. Petrov, V. Shurshakov, V. Benghin, F. Spurny, Calibration Results Obtained With Liulin-4 Type Dosimeters. *Adv. Space Res.* V 30, No 4, 2002, 917-925. [http://dx.doi.org/10.1016/S0273-1177\(02\)00411-8](http://dx.doi.org/10.1016/S0273-1177(02)00411-8).
21. Semkova, J, R. Koleva, G. Todorova, N. Kanchev, V. Petrov, V. Shurshakov, V. Benghin, I. Tchhernykh, Yu. Akatov, V. Redko, Yu. Ivanov, Investigation of dose and flux dynamics in the Liulin-5 dosimeter of the tissue-equivalent phantom onboard the Russian segment of the International Space Station, *Adv. Space Res.*, 31, 2003, 1383-1388.
22. Semkova, J., S. Maltchev, B. Tomov, Yu. Matviichuk, Ts. Dachev, R. Koleva, V. Benghin, I. Chernykh, V. Shurshakov, V. Petrov, Charged particle telescope Liulin-Phobos for radiation environment study during upcoming Phobos Sample Return Mission, *Proceedings of the International Conference on Fundamental Space Research, Sunny Beach, Bulgaria, 23-28 September 2008*, ISBN 978-954-322-316-9, 351-354. Available online at: <http://www.stil.bas.bg/FSR2009/>.
23. Stassinopoulos E.G., C.A. Stauffer, T.P. Dachev, C.J. Brucker, B.T. Tomov, P.G. Dimitrov, The LIULIN-3M Radiometer for Measuring Particle Doses in Space and on Aircraft, NASA/TM-2002-210003, February, 2002. Available online at: http://ntrs.nasa.gov/archive/nasa/casi.ntrs.nasa.gov/20020045343_2002075693.pdf
24. Dachev, Ts.P., B.T. Tomov, Yu.N. Matviichuk, Pl.G. Dimitrov, F. Spurny, O. Ploc, K. Brabkova, I. Jadrnickova, Liulin type spectrometry-dosemetri instruments, *Radiat Prot. Dosimetry*, 2011, 675-679. <http://dx.doi.org/10.1093/rpd/ncq506>

25. Dachev Ts.P., Characterization of near Earth radiation environment by Liulin type instruments. *Adv. Space Res.* 44, 2009, 1441-1449. doi:10.1016/j.asr.2009.08.007.
26. Dachev, Ts.P., F. Spurny, O. Ploc, Characterization of radiation environment by Liulin type spectrometers, *Radiat Prot Dosimetry*, 144 (1-4), 2011, 680-683. <http://dx.doi.org/10.1093/rpd/ncq534>
27. Spurny, F. and Ts. Dachev, Long-Term Monitoring of the Onboard Aircraft Exposure Level With a Si-Diode Based Spectrometer. *Adv. Space Res.*, 32, No.1, 2003, 53-58. [http://dx.doi.org/10.1016/S0273-1177\(03\)90370-X](http://dx.doi.org/10.1016/S0273-1177(03)90370-X)
28. Mitaroff, A., M. Silari, The CERN-EU high energy reference field (CERF) facility for dosimetry at commercial flight altitudes and in space. *Radiat. Prot. Dosim.* 102, 2002, 7–22.
29. Spurny, F., Response of a Si-diode-based device to fast neutrons, *Radiation Measurements* 39, 2005, 219-223. <http://dx.doi.org/10.1016/j.radmeas.2004.05.006>.
30. Ploc, O., F. Spurny, Ts.P. Dachev, Use of Energy Depositing Spectrometer for Individual Monitoring of Aircrew, *Radiat Prot Dosimetry*, 144 (1-4), 2011, 611-614. <http://dx.doi.org/10.1093/rpd/ncq505>
31. Spurny, F., O. Ploc, and I. Jadrníková, Spectrometry of linear energy transfer and dosimetry measurements onboard spacecrafts and aircrafts. *Phys. Part. Nuclei Lett.*, 6, 70–77, # Pleiades Publishing, Ltd. ISSN 2009, 1547-4771.
32. Dachev, Ts., G. Horneck, D.-P. Häder, M. Lebert, P. Richter, M. Schuster, R. Demets, Time profile of cosmic radiation exposure during the EXPOSE-E mission: the R3D instrument. *Journal of Astrobiology*, 12, 5, 2012, 403-411. <http://eea.spaceflight.esa.int/attachments/spacestations/ID501800a9c26c2.pdf>.
33. Berger M.J., J.S. Coursey, M.A. Zucker, and J. Chang, Stopping-Power and Range Tables for Electrons, Protons, and Helium Ions., NIST Standard Reference Database 124. Available online at: <http://physics.nist.gov/PhysRefData/Star/Text/contents.html>.
34. Dachev, Ts.P., B.T. Tomov, Yu.N. Matviichuk, Pl.G. Dimitrov, S V. Vadawale, J.N. Goswami, V. Girish, G. de Angelis, An overview of RADOM results for Earth and Moon Radiation Environment on Chandrayan-1 Satellite, *Adv. Space Res.*, 48, 5, 2011, 779-791. <http://dx.doi.org/10.1016/j.asr.2011.05.009>
35. Uchihori, Y., H. Kitamura, K. Fujitaka, Ts.P. Dachev, B.T. Tomov, P.G. Dimitrov, Y. Matviichuk, Analysis of the calibration results obtained with Liulin-4J spectrometer–dosimeter on protons and heavy ions. *Radiat. Meas.* 35, 2002, 127–134.
36. Uchihori, Y, T. Dachev, H. Kitamura, H. Kentaro, K. Yajima, Chapter VII — Liulin-4J Silicon Portable Spectrometer, Report, HIMAC-078, 2003, 56-63.
37. Zhang, L., R. Mao, R. Zhu, Fast neutron induced nuclear counter effect in Hamamatsu silicon PIN diodes and APDs, *IEEE Transactions on Nuclear Science* 58 (3), 2011, 1249–1256.

38. Burmeister, S., R. Beaujean, F. Petersen, G. Reitz, Post Flight, Calibration of DOSTEL with Heavy Ions During the First and Third, ICCHIBAN, Run at HIMAC, Chiba. 8th Workshop on Radiation Monitoring for the International Space Station 3–5 September 2003, LBNL, Berkeley, USA. Available online at: <http://wrmiss.org/workshops/eighth/burmeister.pdf>
39. Uchihori, Y., H. Kitamura, K. Fujitaka, N. Yasuda, E. Benton, Comparison of results from the 1st ICCHIBAN experiment and current status of the 3rd ICCHIBAN experiment. In: 8th Workshop on Radiation Monitoring for the International Space Station 3–5 September, LBNL, Berkeley, USA, 2003. Available online at: <http://wrmiss.org/workshops/eighth/uchihori.pdf>
40. Zapp, NASA GSFC, by 'Coordinated Data Analysis Web' at Goddard Space Flight Center, May, 2013. <http://cdaweb.gsfc.nasa.gov/tmp/>.
41. Dachev Ts., Analysis of the space radiation doses obtained simultaneously at 2 different locations outside ISS, *Adv. Space Res.*, 52, 2013, 1902-1910. <http://dx.doi.org/10.1016/j.asr.2013.08.011>.
42. Radiation Protection 140, 2004. Cosmic Radiation Exposure of Aircraft Crew, Compilation of Measured and Calculated Data, Edited by L. Lindborg, D.T. Bartlett, P. Beck, I.R. McAulay, K. Schnuer, H. Schraube and F. Spurný, Final Report of EURADOS WG 5, Group of Experts established under Article 31 of the Euratom treaty, Directorate-General for Energy and Transport, Directorate H - Nuclear Energy, Unit H.4 - Radiation Protection Available online at: http://ec.europa.eu/energy/nuclear/radiation_protection/doc/publication/140.pdf
43. Green, A.R., L.G.I. Bennett, B.J. Lewis, F. Kitching, M.J. McCall, M. Desormeaux, A. Butler, An empirical approach to the measurement of the cosmic radiation field at jet aircraft altitudes, *Advances in Space Research*, 36, 2005, 1618-1626.
44. Getley, I. L., L.G.I. Bennett, B.J. Lewis, B. Bennett, C.S. Dyer, A.D.P. Hands, and M.L. Duldig, Evaluation of new cosmic radiation monitors designed for aircrew exposure assessment, *Space Weather*, 8, 2010. S01001. <http://dx.doi.org/doi:10.1029/2009SW000492>.
- 44a. Getley, I. L., Cosmic and solar radiation monitoring of Australian commercial flight crew at high southern latitudes as measured and compared to predictive computer modelling, A Doctoral Thesis Submitted in Fulfilment of the Requirements for the Award of Doctor of Philosophy of The University of New South Wales, June 2007.
45. Semkova, J., R. Koleva, V. Shurshakov, V. Beninghin, St. Maltchev, N. Kanchev, V. Petrov, E. Yarmanova, I. Chernykh, Status and calibration results of Liulin-5 charged particle telescope designed for radiation measurements in a human phantom onboard the ISS, *Advances in Space Research*, 40, 2007, 1586–1592. <http://dx.doi.org/doi:10.1016/j.asr.2007.01.008>.
46. Akatov, Yu.A., V.G. Eremenko, I.S. Kartsev, et al., Spherical phantom for studying radiation conditions in outer space. *Nuclear Measurement & Information Technologies*, 3, 2002, 67-71.
47. Shurshakov, V., Y. Akatov, I.S. Kartsev, et al., Measurements of the absorbed dose distribution in the spherical tissue equivalent phantom in

- MATROSHKA-R space experiment, 11th WRMISS, United Kingdom, Oxford, 2006, Available online at: <http://www.wrmiss.org/workshops/eleveth>
48. Semkova, J., R. Koleva, St. Maltchev et al., Radiation measurements inside a human phantom aboard the International Space Station using Liulin-5 charged particle telescope, *Advances in space research*, 45, Issue 7, 2010, 858-865. <http://dx.doi.org/doi:10.1016/j.asr.2009.08.027>.
 49. Dachev, Ts., J. Semkova, B. Tomov, Y. Matviichuk, P. Dimitrov, N. Bankov, R. Koleva, L. Zelenyi, I. Mitrofanov, A. Malakhov, M. Mokrousov, V. Tretyakov, V. Petrov, V. Shurshakov, V. Benghin, Bulgarian Participation in Future Interplanetary Missions, *Proceedings of Seventh Scientific Conference with International Participation SES*, Sofia, 4-6 December 2012, ISSN 1313-3888, 2013, 55-63. <http://www.space.bas.bg/SES2012/Ph-5.pdf>.
 50. Uchihori Y., E.R. Benton, N. Yasuda, et al., ICCHIBAN Working Group and ICCHIBAN participants NSRL-ICCHIBAN Brief Report, ICCHIBAN-7&8 Announcement and Future ICCHIBAN experiments, 10th WRMISS, Chiba, Japan, 2005. Available online at: http://wrmiss.org/workshops/tenth/pdf/01_uchihori.pdf.
 51. Semkova, J., St. Maltchev, V. Benghin, Y. Uchihori, N. Yasuda, H. Kitamura, Results of Liulin-F particle telescope pre-flight calibrations with protons and heavy ions *Proceedings of Fundamental Space Research conference 2009*, 211-214. <http://www.stil.bas.bg/FSR2009/>.
 52. Dachev, Ts.P. B.T. Tomov, Yu.N. Matviichuk, R.T. Koleva, J.V. Semkova, V.M. Petrov, V.V. Benghin, Yu.V. Ivanov, V.A. Shurshakov, J. Lemaire, Solar Cycle Variations of MIR Radiation Environment as Observed by the LIULIN Dosimeter, *Radiation Measurements*, 30 (3), 1999, 269-274. [http://dx.doi.org/10.1016/S1350-4487\(99\)00061-X](http://dx.doi.org/10.1016/S1350-4487(99)00061-X).
 53. Dachev Ts.P., J.V. Semkova, Yu.N. Matviichuk, B.T. Tomov, R.T. Koleva, P.T. Baynov, V.M. Petrov, V.V. Shurshakov, Yu. Ivanov, Inner Magnetosphere Variations after Solar Proton Events. Observations on Mir Space Station In 1989-1994 Time Period, *Adv. Space Res.*, 22, No 4, 1998, 521-526. [http://dx.doi.org/10.1016/S0273-1177\(98\)01073-4](http://dx.doi.org/10.1016/S0273-1177(98)01073-4).
 54. Shurshakov, V.A., V.M. Petrov, Yu.V. Ivanov, V.A. Bondarenko, V.V. Tzetlin, V.S. Makhmutov, Ts.P. Dachev and J.V. Semkova, Solar particle events observed on MIR station, *Radiation Measurements*, 30, 1999, 317-325. [http://dx.doi.org/10.1016/S1350-4487\(99\)00058-X](http://dx.doi.org/10.1016/S1350-4487(99)00058-X).
 55. Heffner J., Nuclear radiation and safety in space. M, Atomizdat, 1971, pp 115. (in Russian)
 56. Dachev, T., W. Atwell, E. Semones, B. Tomov, B. Reddell, ISS Observations of SAA radiation distribution by Liulin-E094 instrument on ISS, *Adv. Space Res.*, 37, 2006, 1672-1677. doi:10.1016/j.asr.2006.01.001.
 57. Wilson J.W., J.E. Nealy, T. Dachev, B.T. Tomov, F.A. Cucinotta, F.F. Badavi, G. De Angelis, N. Leutke, W.

- Atwell, Time serial analysis of the induced LEO environment within the ISS 6A. *Adv. Space Res.*, 40, 11, 2007, 1562-1570. doi:10.1016/j.asr.2006.12.030.
58. Nealy J.E., F.A. Cucinotta, J.W. Wilson, F.F. Badavi, N. Zapp, T. Dachev, B.T. Tomov, E. Semones, S.A. Walker, G.De Angelis, S.R. Blattnig, W. Atwell, Pre-engineering spaceflight validation of environmental models and the 2005 HZETRN simulation code. *Adv. Space Res.*, 40, 11, 2007, 1593-1610. doi:10.1016/j.asr.2006.12.030.
 59. Slaba, T.C., S.R. Blattnig, F.F. Badavi, N.N. Stoffle, R.D. Rutledge, K.T. Lee, E.N. Zapp, T.P. Dachev and B.T. Tomov, Statistical Validation of HZETRN as a Function of Vertical Cutoff Rigidity using ISS Measurements. *Adv. Space Res.*, 47, 2011, 600-610. doi:10.1016/j.asr.2010.10.021.
 60. Dachev, Ts., B. Tomov, Yu. Matviichuk, Pl. Dimitrov, R. Koleva, J. Semkova, J. Lemaire, V. Petrov, V. Shurshakov, Overview on the MIR radiation environment results obtained by LIULIN instrument in 1988–1994 time period. Description of LIULIN-4 subsystem for the Russian segment of the ISS. In: *Risk Evaluation of Cosmic-ray Exposure in Long-term Manned Space Mission*, Tokyo, Japan, 1999, 127–150.
 61. Semkova, J., R. Koleva, St. Maltchev, N. Bankov, V. Benghin, et al., Depth dose measurements with the Liulin-5 experiment inside the spherical phantom of the Matroshka-R project onboard the International Space Station, *Adv. Space Res.*, 49, 2012, 471–478. <http://dx.doi.org/10.1016/j.asr.2011.10.005>.
 62. Semkova, J., R. Koleva, St. Maltchev, N. Bankov, V. Benghin, et al., Radiation characteristics in the spherical tissue-equivalent phantom on the ISS during solar activity minimum according the data from Liulin-5 experiment, *J. Atm. Solar-Terr. Phys.*, 99, July 2013, 157–163. <http://dx.doi.org/10.1016/j.jastp.2012.07.006>.
 63. Semkova, J., R. Koleva, N. Bankov, St. Malchev, V.M. Petrov, et al., Study of radiation conditions onboard the International space station by means of the Liulin-5 dosimeter, *Cosmic Research*, 51 (2), 2013, 124-132. <http://dx.doi.org/doi:10.1134/S0010952512060068>.
 - 63a. Semkova, J., T. Dachev, R. Koleva, S. Maltchev, N. Bankov, et al., Radiation Environment on the International Space Station During the Solar Particle Events in March 2012, *Astrol. Outreach*, 1, 2013, 102. <http://dx.doi.org/doi:10.4172/jao.1000102>.
 64. Dachev T.P., Semkova J., Tomov B., Matviichuk Yu., Dimitrov Pl., Koleva R., Malchev St., Reitz G., Horneck G., Angelis G. De, Häder D.-P., Petrov V., Shurshakov V., Benghin V., Chernykh I., Drobyshev S., Bankov N. G. Space Shuttle drops down the SAA doses on ISS. *Adv. Space Res.* 47, 2011, 2030-2038. doi:10.1016/j.asr.2011.01.034.
 65. Semones, E., ISS TEPC measurement results, 13th Workshop on Radiation Monitoring for the International Space Station (WRMISS), Krakow, Poland,

- September 8–10, 2008. Available online at: http://wrmiss.org/workshops/thirteenth/Semones_TEPC.pdf.
66. Benghin, V.V., V.M. Petrov, S.G. Drobyshev, M.I. Panasyuk, O.Yu. Nechaev, A.G. Miasnikov, and A.N. Volkov, Results of the radiation monitoring system onboard the service module of ISS, 13th Workshop on Radiation Monitoring for the International Space Station (WRMISS), Krakow, Poland, September 8–10, 2008. Available online at: <http://wrmiss.org/workshops/thirteenth/Benghin.pdf>.
 67. Chernykh, I., Petrov, V., Shurshakov, V., et al., ISS attitude influence on the dose rate measured with Liulin-5 instrument, Workshop on Radiation Measurements on ISS, Krakow, Poland, 8-10 September 2008, <http://www.wrmiss.org/workshops/thirteenth/Chernykh.pdf>.
 68. Dachev, Ts., G. Horneck, D.-P. Häder, M. Schuster, and M. Lebert, EXPOSE-R cosmic radiation time profile, *Jornal of Astrobiology*, available on CJO20142014. http://journals.cambridge.org/article_S1473550414000093.
 69. Dachev T., B. Tomov, Y. Matviichuk, P. Dimitrov, G. De Angelis, Y. Uchihori, O. Ploc, Main Specifications of New Liulin Type Intelligent Crew Personal Dosimeter, Proceedings of Sixth Scientific Conference with International Participation SES, Sofia, ISSN 13131-3888, 2011, 76-82. http://www.space.bas.bg/SENS/SES2010/1_SpPh/10.pdf.
 70. Häder D.P., P. Richter, M. Schuster, Ts. Dachev, B. Tomov, Pl. Dimitrov, Yu. Matviichuk, R3D-B2 - Measurement of ionizing and solar radiation in open space in the BIOPAN 5 facility outside the FOTON M2 satellite, *Adv. Space Res.* 43, 8, 2009, 1200-1211. doi:10.1016/j.asr.2009.01.021.
 - 70a. Damasso M., Ts. Dachev, G. Falzetta, M.T. Giardi, G. Rea, A. Zanini, The radiation environment observed by Liulin-Photo and R3D-B3 spectrum-dosimeters inside and outside Foton-M3 spacecraft, *Radiation Measurements*, V. 44, N0 3, 2009, 263-272. doi:10.1016/j.radmeas.2009.03.007.
 71. Dachev, T.P., B.T. Tomov, Yu.N. Matviichuk, Pl.G. Dimitrov, NG. Bankov, V. V. Shurshakov, O.A. Ivanova, D.-P. Häder, M.T. Schuster, G. Reitz, G. Horneck, “BION-M” №1 spacecraft radiation environment as observed by the RD3-B3 radiometer-dosimeter in April-May 2013, *Journal of Atmospheric and Solar-Terrestrial Physics*, Paper ATP-S-14-00142, 2014. (in print)
 72. Spurny, F., Dosimetry Measurements during a Balloon Flight – June 2000, Report DRD NPI AS CR 488/00, September 2000.
 73. Uchihori, Y., E. Benton, J. Moeller, G. Bendrick, Radiation measurements aboard NASA ER-2 high altitude aircraft with the Liulin-4J portable spectrometer, *Advances in Space Research*, 32, 2003, 41-46.
 74. Ploc, O., Measurement of Exposure to Cosmic Radiation at Near-Earth Vicinity with Energy Deposition Spectrometer Liulin onboard Aircraft and Spacecraft, PhD Thesis, September 2009.
 - 74a. Ploc, O., I. Ambrožová, J. Kubančák, I. Kovář, Ts. Dachev, Publicly available database of measurements with the silicon

- spectrometer Liulin on board aircraft, Radiation measurements, 58, 2013, 107-112. <http://dx.doi.org/10.1016/j.radmeas.2013.09.002>.
75. Friedberg, W., Snyder, W., Faulkner, D.N., US FAA Report DOT/FAA/AM-92-2, 1992.
 76. Sáez Vergara, J.C., and R. Dominguez-Mompell, The implementation of cosmic radiation monitoring in routine flight operation of IBERIA airline of Spain: 1 y of experience of in-flight permanent monitoring, Radiation Protection Dosimetry, 136, 2009, 291-296.
 77. Hwang, J., J. Lee1, K.-S. Cho, H.-S. Choi, S. Rho, and I.-H. Cho, Space Radiation Measurement on the Polar Route onboard the Korean Commercial Flights, J. Astron. Space Sci., 27(1), 2010, 43–54.
 78. Матвийчук, Ю., Димитров Пл., Томов Б., Дачев Цв., Мониторинг радиационной обстановки в реальном масштабе времени с использованием сети Интернет, Proceedings of Fundamental Space Research Conference, 343-346, Slanchev Briag, September 23-28, 2008. http://www.stil.bas.bg/FSR/PDF/TOP5Matviichuk_Yuriy2211249.pdf
 79. Adams, J.H., L. Adcock, J. Apple, M. Christl, W. Cleveand, M. Cox, K. Dietz, C. Ferguson, W. Fountain, B. Ghita, E. Kuznetsov, M. Milton, J. Myers, S. O'Brien, J. Seaquist, E. A. Smith, G. Smith, L. Warden and J. Watts, Nuclear Instruments and Methods in Physics Research Section A: Accelerators, Spectrometers, Detectors and Associated Equipment, 579, 2007, 522-525.
 80. Grigoriev, A. V., O. R. Grigoryan, A. Y. Drozdov, Y. M. Malyshkin, Y. V. Popov, E. A. Mareev, and D. I. Iudin Thunderstorm neutrons in near space: Analyses and numerical simulation, J. Geophys. Res., 2010, 115, A00E52, doi:10.1029/2009JA014870.
 81. Petrov V.L., M.I. Panasyuk, A.M. Amelyushkin, A.Yu. Drozdov, O.Yu. Nechaev, RAZREZ system for RADIOSCAF experiment, Fourteenth WRMISS Workshop, Dublin, UK, 7–9 September 2010. Available online at: <http://www.wrmiss.org/workshops/fourteenth/Petrov.pdf>.
 82. Tomov B., Pl. Dimitrov, Yu. Matviichuk, Ts. Dachev, Galactic and Solar Cosmic Rays Study by Ground and Rocketborne Space Radiation Spectrometers-Dosimeters- Liulin-6R and Liulin-R, Proceedings of Fundamental Space Research Conference, ISSN 978-954-322-316-9, 2008, 252-257. , http://www.stil.bas.bg/FSR/PDF/TOP5Tomov_Borislav2242058.pdf.
 83. Wissmann, F., O. Burda, S. Khurana, T. Klages, and F. Langner, Dosimetry of secondary cosmic radiation up to an altitude of 30 km, Radiat. Prot. Dosimetry, First published online December 16, 2013. doi:10.1093/rpd/nct329.
 84. Kitching, F., Use of a Liulin Detector for the Determination of Aircrew Radiation Exposure, Master's Thesis, Royal Military College of Canada, Kingston, Ont., Canada, November 2004.
 85. Dachev, T.P., Profile of the ionizing radiation exposure between the Earth surface and free space, Journal of Atmospheric and Solar-Terrestrial Physics, 102, September 2013, 148–156, 2013. <http://dx.doi.org/10.1016/j.jastp.2013.05.015>

ОПИСАНИЕ НА ПРИБОРИТЕ ОТ ТИПА „ЛЮЛИН“ И ГЛАВНИ НАУЧНИ РЕЗУЛТАТИ

*Цв. Дачев, Й. Семкова, Б. Томов, Ю. Матвийчук,
Пл. Димитров, Н. Банков, Р. Колева, Ст. Малчев*

Резюме

Йонизиращата радиация създава здравни проблеми за хората на повърхността, в атмосферата и в околоземното космическо пространство. Оценката на радиационното въздействие върху здравето изисква точно познаване на натрупаната погълната доза, която зависи от глобалното разпределение на космическата радиация, фазата на слънчевия цикъл и от локалните вариации, генерирани от разпределението на масата около точката на измерване. В статията е направен обзор на създадените в България спектрометри-дозиметри от типа „Люлин“ и основните научни резултати, които са получени с тях от 1988 г. досега на самолети, балони, ракети и спътници, включително станцията „Мир“ и международната космическа станция (МКС).